CHALMERS

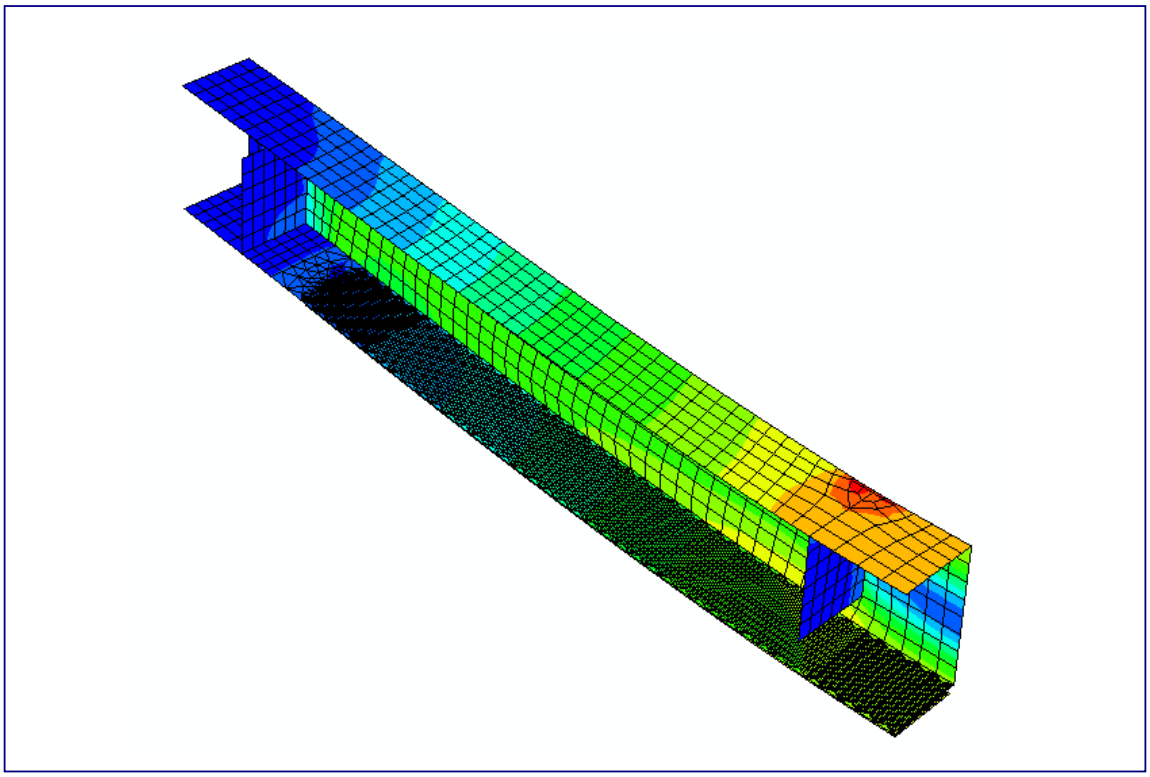

Finite Element Modelling of Adhesive Interface between Steel and CFRP

Master's Thesis in the International Master's Programme in structural Engineering

ABU THOMAS ZACHARIAH

Department of Civil and Environmental Engineering
Division of Civil Engineering
Steel and Timber Structures
CHALMERS UNIVERSITY OF TECHNOLOGY
Göteborg, Sweden 2006
Master's Thesis 2006:61

MASTER'S THESIS 2006:61

Finite Element Modelling of Adhesive Interface between Steel and CFRP

Master's Thesis in the International Master's Programme in structural Engineering

ABU THOMAS ZACHARIAH

Department of Civil and Environmental Engineering
Division of Civil Engineering
Steel and Timber Structures
CHALMERS UNIVERSITY OF TECHNOLOGY

Göteborg, Sweden 2006

Finite Element Modelling of Adhesive Interface between Steel and CFRP

Master's Thesis in the International Master's Programme in structural Engineering
ABU THOMAS ZACHARIAH

Master's Thesis 2006:61
Department of Civil and Environmental Engineering
Division of Civil Engineering
Steel and Timber Structures
Chalmers University of Technology
SE-412 96 Göteborg
Sweden
Telephone: + 46 (0)31-772 1000

Cover:
Longitudinal stress distribution at 170 kN load on composite beam modelled with 2D shell elements and spring connectors for the adhesive layer.

Department of Civil and Environmental Engineering
Göteborg, Sweden 2006

Finite Element Modelling of Adhesive Interface between Steel and CFRP
Master's Thesis in the International Master's Programme in structural Engineering

ABU THOMAS ZACHARIAH
Department of Civil and Environmental Engineering
Division of Civil Engineering
Steel and Timber Structures
Chalmers University of Technology

ABSTRACT

CFRP has been an interesting alternative while it comes to rehabilitation and repair work of structures whether made of concrete or steel. However since the combination of CFRP and the latter is more recent there has been a need to think of the best way to model the adhesive interface between the two in a composite beam.

The initial task was to make a lighter FE model (less use of 3D solid elements) of the laboratory set-up so that the results obtained from tests, conducted in the laboratory, could be verified. Also for the purpose of comparison, the results from a high detail 3D solid element FE model, as part of the ongoing PhD research of Dag Linghoff was available.

The present model was created with 2D shell elements and spring connectors to model the adhesive interface, as it was a more easily applicable solution. Difficulties were faced during the process of modelling the interface since ABAQUS® the general purpose FE tool used did not have such an option to use spring connectors as a modelling element for the adhesive. Yet the model was constructed successfully and a method to extract the results from it was found out.

The results from the model showed an excellent agreement to the analytical interfacial shear stresses, though the process of result extraction was very complicated and laborious. However it was not possible to study the normal (peeling) stresses in this way since the method involved an almost manual process of calculating the peeling stress.

The model is very easy to create on simple 2D surfaces but would be get extremely complicated when there would be 3D adhesive layer shape. The process would then have to be built into the software as a function for easy use by just selection of surfaces rather than manual set up.

Key words: Adhesive interface, CFRP-Steel composite, Epoxy modelling, Finite element modelling, ABAQUS®, interfacial Shear stresses, Spring Connectors

Finit Element modellering av limfog mellan stål och kolfiberarmerad polymer

Examensarbete inom konstruktionsteknik

ABU THOMAS ZACHARIAH
Institutionen för bygg- och miljöteknik
Avdelningen för konstruktionsteknik
Stål- och träbyggnad
Chalmers tekniska högskola

SAMMANFATTNING

CFRP är ett interessant alternativ när det kommer till återställande och reparation av byggnader, både när det gäller betong och stål. Eftersom kombinationen av CFRP och det sistnämnda är nyare, har det varit nödvändigt att fundera över det bästa sättet att modellera limmet mellan dessa två i en sammansatt balk.

Den första uppgiften var att göra en lättare FE modell (mindre användning av solida 3D element) av labratorie-strukturen så att resutaten från laborationerna, kunde verifieras. Resultaten från en hög detalj 3D solida element FE modell, från en del av den pågående PhD forskningen av Dag Linghoff, användes för jämförelse. Den nuvarande modellen är framställd med 2D skal element och fjäderkopplingar för att modellera limmet mellan materialen, eftersom detta var en enkel och användbar lösning. Svårigheter dök upp under modelleringen eftersom ABAQUS®, FE hjälpmedlet som använts, inte hade något alternativ för fjäderkopplingar som ett modellerande element för limmet. Modellen kunde ändå konstrueras med framgång och en metod för att få fram resultaten hittades.

Resultaten från modellen visade en bra överensstämmelse med den analytiska skjuvningen mellan materialen, även fast processen för att få fram resultaten var komplicerad. Det var dock inte möjligt att studera normalspänningarna pga. att modellen involverade en nästan helt manuell process för att beräkna normalspänningarna.

Modellen är väldigt enkel att skapa med 2D ytor, men skulle bli väldigt komplicerad om man använde sig utav 3D. Den processen skulle behövts byggas in i mjukvaran som en funktion för lätt användning bara med valfrihet av yta hellre än manuell uppbyggnad.

Nyckelord: Limfog, CFRP-stål komposit, epoxi modellering, Finite element modellering, ABAQUS, skjuvspänningar i limfog, fjäder förbindning

Contents

Preface

This master thesis is a part of an experimental research on composite reinforcement that is being carried out at various universities around Europe. The main goals of the programme is to research in the field of FRP, set standards, scientific processes and encourage its use in the industry.

The master thesis was carried out between January 2006 and June 2006 at the Department of Structural Engineering, Steel and timber structures, Chalmers University of Technology, Sweden.

I would like to express my gratitude to my supervisor, researcher Dag Linghoff, M.Sc for his unconditional support and guidance and the very valuable advising of the esteemed examiner Dr. Mohammed Al-Emrani.

I would also like to thank the course coordinator, Prof. Björn Engström, M.Sc.,C.E.,Ph.D for his support and cooperation.

I also appreciate the valuable comments of my opponent Olga Lucia Garzon.

Finally, I could not have completed this thesis with out the support of my parents and my friends.

Göteborg June 2006

Abu Thomas Zachariah

Notations

Roman upper case letters

A_1	Area of adherent 1
A_2	Area of adherent 2
A_{CFRP}	Area of CFRP Laminate
A_s	Area of steel
B	Breadth of element
D_{11}	Elastic relative stiffness along the first axis
D_{22}	Elastic relative stiffness along the second axis
E_1	Young's Modulus of Elasticity of adherent 1
E_2	Young's Modulus of Elasticity of adherent 2
E_{CFRP}	Young's Modulus of Elasticity of CFRP
E_S	Young's Modulus of Elasticity for Steel
F	Force
G_a	Shear Modulus of Elasticity
H	Height of Element
$I_{CFRP.el}$	Moment of Inertia of composite section with CFRP
$I_{el.no\_CFRP}$	Moment of Inertia of composite section without CFRP
L	Length of the element
LS1	Longitudinal normal stress at point 1
M	Moment applied
N	Axial load
P	Point load applied
R	Ratio of the elastic stiffness

Roman lower case letters

b_1	Breadth of adherent 1
b_2	Breadth of adherent 1
b_{CFRP}	Breadth of CFRP laminate
h_{CFRP}	Height of CFRP laminate
u	Displacement along x-axis
v	Displacement along y-axis
w	Displacement along z-axis
x	Co-ordinate along x-axis
y	Co-ordinate along y-axis
z	Co-ordinate along z-axis

Greek lower case letters

α	Constant
β	Constant
ε	Strain
γ	Strain
σ	Stress
τ	Shear stress

1 Introduction

Man has always wanted to better what he has done so far and as a step towards this he tries to stretch all that he can to its limits. When he knows he cannot go any further with what he has, he tends to replace it. But replacement is not always a solution, one can also modify what already exists to suit the needs of the day and this is definitely a more cost effective way than replacement. One could like in this case, as is the subject of study, use CFRP (Carbon fibre Reinforced Polymer) strips to reinforce or strengthen the existing member. But further study on this is required so as to understand how this composite member would react to loads. It is also necessary to know what improvements made to the composite member would optimize its performance while keeping in mind the economic feasibility. For this the present thesis would deal with the Modelling of the experimental composite member for Finite Element Analysis.

This chapter will give the reader some information about the background of the present study as well as the aim, objectives and its limitations. A general description of the main method that has been adopted is also given, together with an overview of the earlier research.

1.1 Background

A lot of work in this field has been done and among them the works by Bogdanovich & Kizhakethara [1] prove enlightening, this paper deals with the sub-modelling approach of dealing with modelling composite materials. Then there is the earlier work of Wu and Crocombe [2] who have dealt with the simplified approach of modelling adhesive joints of composite material. From their works we can see how the task of strengthening the steel beam with CFRP has been carried out. The setup is loaded and tested not only in the ULS but also for its deformations in the service state.

1.2 Aim and Objectives

The Aim of the project is to model the interface between the CFRP and steel beam for Finite Element Analysis in ABAQUS. The experimental analysis has been made earlier so now the exact same conditions have to be simulated in ABAQUS so that the results match with those from the experiments and they would also have to be cross checked analytically.

The completion of this master's thesis will lead to better understanding of how to model the interaction between the adhesive and metal and composite adherends.

1.3 Limitations

This thesis has a few limitations like in the case of comparison with or to the results from the laboratory, the tests in the laboratory though have been carried out by the predecessors researchers of this project yet not much of the details from them will be used for this thesis and it will be out of the scope.

2 Literature Study

The literature study was done with an extensive search of journals, papers and other reading material which deals with the state of the art information connected to the subject and which could contribute to the project and so the study was categorized into the following headings.

2.1 Carbon Fibre Reinforced Polymer (CFRP)

The Encyclopaedia defines CFRP as:

Carbon fibre reinforced Plastic (CFRP), is a strong, and light composite material or fibre reinforced polymer. Like glass-reinforced plastic, the composite material is commonly referred to by the name of its reinforcing fibres (carbon fibre). The polymer is most often epoxy, but others plastics, like polyester or vinyl ester, are also sometimes used.

There are many ways to manufacture CFRP out of which the most important continuous manufacturing process is Pultrusion, which we will discuss in brief now and is described in Norling [3].

In this method continuous fibre reinforcement is impregnated with a resin and then continuously formed into a solid composite profile. The fibres are pulled in creels and are gradually brought together and pulled into an open resin bath where the fibres are impregnated with resin. After that the fibres pass though a die where all excess resin is squeezed out and the die is heated and this heat is transferred to the resin to initiate the hardening process. The fibres emerge from the other end of the die as a hot solid composite profile and it is allowed to cool off before being cut into required lengths.

Altenbach and Kissing [4] point that the modelling of this fibre can be done in three stages in which the first level is in the micro level (individual fibre layer orientation is taken into consideration) and then in the macro level (averages values of the parameters in question are taken) and finally in the structural level or global level which is more important for us at a structural point of view. Here the mechanical response of structural members like beams, plates, and shells etc. have to be analysed taking into account possibilities to formulate structural theories of different order.

The Classic Laminate Theory (CLT)[1] is commonly used along with First-order Shear Deformation Theory (FSDT) and Equivalent Single Layer Theory (ESLT). But CLT requires C1 continuity of transverse displacement i.e. the displacements and the derivatives must be continuous while FSDT only requires C0 continuity.

Basic assumption of the modelling structural elements in the framework of anisotropic elasticity is an approximate expression of the displacement components in the form of polynomials are limited to third degree and can be written in the form:

[1] The concept of CLT is not used in present project. However it is presented for better understanding of the concept for future extension of this project.

$$u_1(x_1,x_2,x_3)=u(x_1,x_2)+\alpha x_3\frac{\partial w(x_1,x_2)}{\partial x_1}+\beta x_3\psi_1(x_1,x_2)+\gamma {x_3}^2\phi_1(x_1,x_2)+\delta {x_3}^3\chi_1(x_1,x_2)$$

$$u_2(x_1,x_2,x_3)=v(x_1,x_2)+\alpha x_3\frac{\partial w(x_1,x_2)}{\partial x_2}+\beta x_3\psi_2(x_1,x_2)+\gamma {x_3}^2\phi_2(x_1,x_2)+\delta {x_3}^3\chi_2(x_1,x_2)$$

$$u_3(x_1,x_2,x_3)=w(x_1,x_2)+\overline{\beta}x_3\psi_3(x_1,x_2)+\overline{\gamma}{x_3}^2\phi_3(x_1,x_2)$$

(2.1)

According to the CLT the values of the constants in the above equations will be

$$\alpha=-1,\qquad \beta=\gamma=\delta=\overline{\beta}=\overline{\gamma}=0$$

According to the FSDT the values of the same constants would be

$$\alpha=0,\qquad \beta=1,\qquad \gamma=\delta=\overline{\beta}=\overline{\gamma}=0$$

So the same *Equation (2.1)* would be reduced in the CLT or FSDT as

$$u_1(x_1,x_2,x_3)=u(x_1,x_2)+x_3\psi_1(x_1,x_2)$$

$$u_1(x_1,x_2,x_3)=v(x_1,x_2)+x_3\psi_2(x_1,x_2)$$

(2.2)

$$u_3(x_1,x_2,x_3)=w(x_1,x_2)$$

where

$$\psi_1(x_1,x_2)=-\frac{\partial w}{\partial x_1},\psi_2(x_1,x_2)=-\frac{\partial w}{\partial x_2},$$

The above equations yield the classical approximation and the number of unknown functions reduces to three unknown functions, which are u, v and w.

$$\varepsilon_1=\frac{\partial u}{\partial x_1}+x_3\frac{\partial \psi_1}{\partial x_1},\varepsilon_2=\frac{\partial v}{\partial x_2}+x_3\frac{\partial \psi_2}{\partial x_2},\varepsilon_3=0$$

$$\varepsilon_4=\frac{\partial w}{\partial x_2}+\psi_2,\varepsilon_5=\frac{\partial w}{\partial x_1}+\psi_1$$

$$\varepsilon_6=\frac{\partial u}{\partial x_2}+\frac{\partial v}{\partial x_1}+x_3\left(\frac{\partial \psi_2}{\partial x_1}+\frac{\partial \psi_1}{\partial x_2}\right)$$

(2.3)

For in-plane strains one can write in contracted form

$$\varepsilon_1(x_1,x_2,x_3)=\varepsilon_i(x_1,x_2)+x_3k(x_1,x_2),(i=1,2,6)$$

i.e. the in place strains ε_1, ε_2 and ε_6 vary linearly through thickness h. The stress strain relations in axis coordinates are

$$\sigma_i'=c_{ij}'\varepsilon_j',i,j=1,2,6$$

Using transformation rule,

$$C=T^{3\varepsilon T}CT^{3\varepsilon}$$

CLT makes the additional assumptions

- All layers are in a state of plane stress i.e. $\sigma_3=\sigma_4=\sigma_5=0$
- Normal distances from the middle surface remain constant. i.e. the transverse normal strain ε_3 is negligible compared with the in plane strains ε_1, ε_2
- The transverse shear strains ε_4 and ε_5 are negligible. This assumption implies that straight lines normal to the middle surface remain straight and normal to that surface after deformation.

$\therefore$ *Equation (2.3)* becomes with above assumptions as

$$\psi_1(x_1,x_2)=\frac{-\partial w}{\partial x_1},\psi_2(x_1,x_2)=\frac{-\partial w}{\partial x_2} \tag{2.4}$$

and the displacement approach in *Equation (2.2)* and the strain components in *Equation (2.3)* are written by

$$\begin{aligned}
&u_1(x_1,x_2,x_3)=u(x_1,x_2)-x_3\frac{\partial w(x_1,x_2)}{\partial x_1}\\
&u_2(x_1,x_2,x_3)=v(x_1,x_2)-x_3\frac{\partial w(x_1,x_2)}{\partial x_2}\\
&u_3(x_1,x_2,x_3)=w(x_1,x_2)
\end{aligned} \tag{2.5}$$

$$\begin{aligned}
&\varepsilon_1=\frac{\partial u}{\partial x_1}-x_3\frac{\partial w^2}{\partial {x_1}^2},\varepsilon_2=\frac{\partial v}{\partial x_2}-x_3\frac{\partial w^2}{\partial {x_2}^2},\\
&\varepsilon_3=0,\varepsilon_4=0,\varepsilon_5=0,\\
&\varepsilon_6=\frac{\partial u}{\partial x_2}+\frac{\partial v}{\partial x_1}-2x_3\left(\frac{\partial w^2}{\partial x_1\partial x_2}\right)
\end{aligned} \tag{2.6}$$

The condensed form for in-plane strain can be noted as

$$\varepsilon_1(x_1, x_2, x_3) = \varepsilon_i(x_1, x_2) + x_3(k_1), (i = 1, 2, 6)$$

with

$$\varepsilon_1 = \frac{\partial u}{\partial x_1}, \varepsilon_2 = \frac{\partial v}{\partial x_2},$$
$$\varepsilon_6 = \frac{\partial u}{\partial x_2} + \frac{\partial v}{\partial x_1} \qquad (2.7)$$
$$k_1 = \frac{-\partial w^2}{\partial x_1^2}, k_2 = \frac{-\partial w^2}{\partial x_2^2}, k_1 = \frac{-2\partial w^2}{\partial x_1 \partial x_2}$$

$\varepsilon^T = [\varepsilon_1 \quad \varepsilon_2 \quad \varepsilon_6]$ is the vector of mid plain strains (stretching and shearing) &

$k^T = [k_1 \quad k_2 \quad k_6]$ is the vector of curvature (bending & twisting)

For all k layers

$$\sigma_1^{(k)} = Q_{ij}^{(k)} \varepsilon_i + x_3 Q_{ij}^{(k)} k_{ij}$$
$$here \qquad (2.8)$$
$$i, j = 1, 2, 6$$

2.2 Adhesives and its failure

The adhesives are used to make the CFRP adhere to the steel member and it is also the medium through which the forces are transferred from the steel to the CFRP strips.

There are many types of adhesives and the type of adhesive used in the present analysis is the plastic epoxy with a Young's Modulus of 7 GPa and a Poisson's ratio of 0.29. The commercial name of this epoxy is Sikadur®. During the analysis in this thesis it will assumed that the epoxy is linear elastic.

Adhesives may fail in one of two ways:

- *Adhesive failure* is the failure of the adhesive to stick or bond with the material to be adhered (also known as the substrate or adherend).
- *Cohesive failure* is structural failure of the adhesive. Adhesive remains on both substrate surfaces, but the two items separate.

Two substrates can also separate through structural failure of one of the substrates, this is not a case of failure of the adhesive. The adhesive remains intact and is still bonded to one substrate and the remnants of the other.

2.3 Interfacial Stresses in Composite Beams

Smith and Teng [5] have formulated the interfacial stresses in their paper on *Interfacial Stresses in Plated Beams*. There were many existing solutions but most of them were either inaccurate or not valid in all load cases and also complex. So the new solution took into effect the bending deformations in the plate and the axial deformations in the beam.

The new solution uses the following assumptions, and the solution is described in terms of adherents 1 and 2, where adherent 1 is the beam and adherent 2 is the soffit plate. Adherent 2 can be either steel or FRP but not limited to these two. Linear elastic behaviour of adherents 1 and 2, as well as of the adhesive layer, is assumed. Deformations of adherents 1 and 2 are due to bending moments, axial and shear forces. The adhesive layer is assumed to be subject to stresses invariant across its thickness. This is the key assumption, which enables us to obtain relatively simple closed-form solutions. Under normal stresses in the thickness wise direction, the adhesive layer will deform, so the vertical displacements at the bottom of adherent 1 and the top of adherent 2 differ. As a result, the curvature of the beam will differ from that of the soffit plate. These thickness wise deformations of the adhesive are assumed to have a negligible effect on the interfacial shear stresses. That is, in finding the interfacial shear stresses, the curvatures of both adherents are assumed to be the same. This assumption is not used in the determination of interfacial normal stresses.

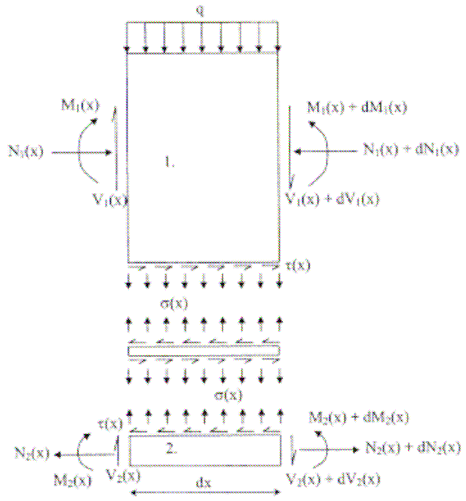

Figure 2.1 Differential segment of a soffit-plated beam.

2.3.1 Governing differential equation for the interfacial stresses

The governing differential equation for the interfacial stresses can be derived as followed. A differential segment of a plated beam is shown in *Figure 2.1*, where the interfacial shear and normal stresses are denoted by $\tau(x)$ and $\sigma(x)$, respectively. *Figure 2.1* also shows the positive sign convention for the bending moment, shear force, axial force and applied loading. The shear strain γ in the adhesive layer can be written as

$$\gamma = \frac{du(x,y)}{dy} + \frac{dv(x,y)}{dx} \tag{2.9}$$

Where $u(x, y)$ and $v(x, y)$ are the horizontal and vertical displacements respectively at any point in the adhesive layer. The corresponding shear stress is given as

$$\tau(x) = G_a\left(\frac{du(x,y)}{dy} + \frac{dv(x,y)}{dx}\right) \tag{2.10}$$

Where G_a is the shear modulus of the adhesive layer. Differentiating the above expression with respect to x gives

$$\frac{d\tau(x)}{dx} = G_a\left(\frac{d^2u(x,y)}{dxdy} + \frac{d^2v(x,y)}{dx^2}\right) \tag{2.11}$$

The curvature of a differential element can be related to the applied moment, $M_T(x)$, by the following

$$\frac{d^2v(x)}{dx^2} = -\frac{1}{(EI)_t}M_T(x) \tag{2.12}$$

Where $(EI)_t$ is the total flexural rigidity of the composite section considering the partial interaction between the two adherents. The adhesive layer is assumed to be subjected to uniform shear stresses and therefore $u(x, y)$ must vary linearly across the adhesive thickness t_a, then

$$\frac{du}{dy} = \frac{1}{t_a}\left[u_2(x) - u_1(x)\right] \tag{2.13}$$

and

$$\frac{d^2u(x,y)}{dxdy} = \frac{1}{t_a}\left[\frac{du_2(x)}{dx} - \frac{du_1(x)}{dx}\right] \tag{2.14}$$

Where $u_1(x)$ and $u_2(x)$ are the longitudinal displacements at the base of adherent 1 and the top of adherent 2, respectively, and t_a is the thickness of the adhesive layer. *Equation (2.11)* can be rewritten using *Equation (2.12)* and *Equation (2.14)*as

$$\frac{d\tau(x)}{dx} = \frac{G_a}{t_a}\left(\frac{du_2(x)}{dx} - \frac{du_1(x)}{dx} - \frac{t_a}{(EI)_t}M_T(x)\right) \tag{2.15}$$

In calculating $(EI)_t$, interfacial shear stresses should be considered but to do so would complicate the solution. The third term in parentheses in *Equation (2.15)* is very small and thus is ignored in the following derivation. The strains at the base of adherent 1 and the top of

adherent 2, considering all three components of axial, bending and shear deformations, are given as

$$\varepsilon_1(x) = \frac{du_1}{dx} = \frac{y_1}{E_1 I_1} M_1(x) - \frac{1}{E_1 A_1} N_1(x) + \frac{y_1}{G_1 \alpha A_1} \left[q + b_2 \sigma(x) \right] \tag{2.16}$$

and

$$\varepsilon_2(x) = \frac{du_2}{dx} = \frac{y_2}{E_2 I_2} M_2(x) - \frac{1}{E_2 A_2} N_2(x) + \frac{y_2}{G_2 \alpha A_2} \left[b_2 \sigma(x) \right] \tag{2.17}$$

Where E is the elastic modulus, G the shear modulus, b_2 the width of the soffit plate, A the cross-sectional area, I the second moment of area and α is the effective shear area multiplier, which is equal to 5/6 for a rectangular section. The subscripts 1 and 2 denote adherents 1 and 2, respectively. $M(x)$, $N(x)$ and $V(x)$ are the bending moment, axial and shear forces in each adherent while y_1 and y_2 are the distances from the bottom of adherent 1 and the top of adherent 2 to their respective centroid. Consideration of horizontal equilibrium gives

$$\frac{dN_1(x)}{dx} = \frac{dN_2(x)}{dx} = b_2 \tau(x) \tag{2.18}$$

where

$$N_1(x) = N_2(x) = N(x) = b_2 \int_0^x \tau(x) dx \tag{2.19}$$

Assuming equal curvature in the beam and the soffit plate, the relationship between the moments in the two adherents can be expressed as

$$M_1(x) = R M_2(x) \tag{2.20}$$

With,

$$R = \frac{E_1 I_1}{E_2 I_2} \tag{2.21}$$

Moment equilibrium of the differential segment of the plated beam in *Figure 2.1* gives

$$M_T(x) = M_1(x) + M_2(x) + N(x)(y_1 + y_2 + t_a) \tag{2.22}$$

The bending moment in each adherent, expressed as a function of the total applied moment and the interfacial shear stress, is given as

$$M_1(x) = \frac{R}{R+1} \left[M_T(x) - b_2 \int_0^x \tau(x)(y_1 + y_2 + t_a) dx \right] \tag{2.23}$$

$$M_2(x) = \frac{1}{R+1}\left[M_T(x) - b_2 \int_0^x \tau(x)(y_1 + y_2 + t_a)dx \right] \tag{2.24}$$

The first derivative of the bending moment in each adherent gives

$$\frac{dM_1(x)}{dx} = V_1(x) = \frac{R}{R+1}\left[V_T(x) - b_2\tau(x)(y_1 + y_2 + t_a)\right] \tag{2.25}$$

$$\frac{dM_2(x)}{dx} = V_2(x) = \frac{1}{R+1}\left[V_T(x) - b_2\tau(x)(y_1 + y_2 + t_a)\right] \tag{2.26}$$

Substituting *Equation (2.16)* and *Equation (2.17)* into *Equation (2.15)* and differentiating the resulting equation once yields

$$\frac{d^2\tau(x)}{dx^2} = \frac{G_a}{t_a}\begin{pmatrix} -\dfrac{y_2 dM_2(x)}{E_2 I_2 dx} + \dfrac{dN_2(x)}{E_2 A_2 dx} + \dfrac{y_2}{G_2\alpha A_2} b_2 \dfrac{d\sigma(x)}{dx} \\ -\dfrac{y_1 dM_1(x)}{E_1 I_1 dx} + \dfrac{dN_1(x)}{E_1 A_1 dx} - \dfrac{y_1 dq}{G_1\alpha A_1 dx} - \dfrac{y_1}{G_1\alpha A} b_2 \dfrac{d\sigma(x)}{dx} \end{pmatrix} \tag{2.27}$$

Substitution of the shear forces [*Equation (2.25)* and *Equation (2.26)*] and axial forces [*Equation (2.19)*] in both adherents into *Equation (2.27)* gives the following governing differential equation for the interfacial shear stress

$$\begin{aligned} &\frac{d^2\tau(x)}{dx^2} - \frac{G_a b_2}{t_a}\left(\frac{(y+y)(y+y+t)}{EI+EI} + \frac{1}{EA} + \frac{1}{EA}\right)\tau(x) = \\ &-\frac{G}{t}\left(\frac{y+y}{EI+EI}\right)V(x) - \frac{Gydq}{tG\alpha Adx} - \frac{Gb}{\alpha t}\left(\frac{y}{GA} - \frac{y}{GA}\right)\frac{d\sigma(x)}{dx} \end{aligned} \tag{2.28}$$

2.3.2 Governing differential equation for the interfacial normal stresses

The governing differential equation for the interfacial normal stress is derived in this section. When the beam is loaded, vertical separation occurs between adherents 1 and 2. This separation creates an interfacial normal stress in the adhesive layer. The normal stress, s(x), is given as

$$\sigma(x) = \frac{E_a}{t_a}\left[v_2(x) - v_1(x)\right] \tag{2.29}$$

Where $v_1(x)$ and $v_2(x)$ are the vertical displacements of adherents 1 and 2, respectively. The equilibrium of adherents 1 and 2, neglecting second-order terms, leads to the following relationships.

Adherent 1:

$$\frac{d^2 v_1(x)}{dx^2} = -\frac{1}{E_1 I_1} M_1(x) - \frac{1}{G_1\alpha A_1}\left[q + b_2\sigma(x)\right] \tag{2.30}$$

$$\frac{dM_1(x)}{dx} = V_1(x) - b_2 y_1 \tau(x) \tag{2.31}$$

and

$$\frac{dV_1(x)}{dx} = -b_2\sigma(x) - q \tag{2.32}$$

Adherent 2:

$$\frac{d^2 v_2(x)}{dx^2} = -\frac{1}{E_2 I_2} M_2(x) - \frac{1}{G_2 \alpha A_2}\left[b_2\sigma(x)\right] \tag{2.33}$$

$$\frac{dM_2(x)}{dx} = V_2(x) - b_2 y_2 \tau(x) \tag{2.34}$$

and

$$\frac{dV_2(x)}{dx} = -b_2\sigma(x) \tag{2.35}$$

Based on the above equilibrium equations, the governing differential equations for the deflections of adherents 1 and 2, expressed in terms of the interfacial shear and normal stresses, are given as follows.

Adherent 1:

$$\frac{d^4 v_1(x)}{dx^4} = \frac{1}{E_1 I_1} b_2 \sigma(x) - \frac{1}{G_1 \alpha A_1} b_2 \frac{d^2\sigma(x)}{dx^2} + \frac{y_1}{E_1 I_1} b_2 \frac{d\tau(x)}{dx} + \frac{1}{E_1 I_1} q - \frac{d^2 q}{G_1 \alpha A_1 dx^2} \tag{2.36}$$

Adherent 2:

$$\frac{d^4 v_2(x)}{dx^4} = -\frac{1}{E_2 I_2} b_2 \sigma(x) + \frac{1}{G_2 \alpha A_2} b_2 \frac{d^2\sigma(x)}{dx^2} + \frac{y_2}{E_2 I_2} b_2 \frac{d\tau(x)}{dx} \tag{2.37}$$

Substitution of *Equation (2.36)* and *Equation (2.37)* into the fourth derivative of the interfacial normal stress obtainable from *Equation (2.29)* gives the following governing differential equation for the interfacial normal stress

$$\begin{aligned} &\frac{d^4\sigma(x)}{dx^4} - \frac{E_a b_2}{\alpha t_a}\left(\frac{1}{G_1 A_1} + \frac{1}{G_2 A_2}\right)\frac{d^2\sigma(x)}{dx^2} + \frac{E_a b_2}{t_a}\left(\frac{1}{E_1 I_1} + \frac{1}{E_2 I_2}\right)\sigma(x) \\ &= -\frac{E_a b_2}{t_a}\left(\frac{y_1}{E_1 I_1} - \frac{y_2}{E_2 I_2}\right)\frac{d\tau(x)}{dx} - \frac{E_a 1}{t_a E_1 I_1} q + \frac{E_a d^2 q}{t_a G_1 \alpha A_1 dx^2} \end{aligned} \tag{2.38}$$

2.3.3 The final solution Equations for the interfacial stresses

The governing differential equations for the interfacial shear and normal stress [*Equation (2.28)* and *Equation (2.38)*] are coupled and hence a solution is not easily found. To uncouple the equations, the effects of shear deformations in both adherends are now neglected. The governing differential equation for the interfacial shear stress then reduces to

$$\frac{d^2\tau(x)}{dx^2} - \frac{G_a b_2}{t_a}\left(\frac{(y_1+y_2)(y_1+y_2+t_a)}{E_1I_1+E_2I_2} + \frac{1}{E_1A_1} + \frac{1}{E_2A_2}\right)\tau(x) + \frac{G_a}{t_a}\left(\frac{y_1+y_2}{E_1I_1+E_2I_2}\right)V_T(x) = 0 \quad (2.39)$$

For simplicity, the general solutions presented below are limited to loading which is either concentrated or uniformly distributed over part or the whole span of the beam, or both. For such loading, $d^2V_T(x)/dx^2=0$, and the general solution to *Equation (2.39)* is given by

$$\tau(x)=B_1\cosh(\lambda x)+B_2\sinh(\lambda x)+m_1V_T(x) \quad (2.40)$$

Where

$$\lambda^2 = \frac{G_a b_2}{t_a}\left(\frac{(y_1+y_2)(y_1+y_2+t_a)}{E_1I_1+E_2I_2} + \frac{1}{E_1A_1} + \frac{1}{E_2A_2}\right) \quad (2.41)$$

$$m_1 = \frac{G_a 1}{t_a\lambda^2}\left(\frac{y_1+y_2}{E_1I_1+E_2I_2}\right) \quad (2.42)$$

The governing differential equation for the normal stress, with the effects of shear deformations neglected, becomes

$$\frac{d^4\sigma(x)}{dx^4} + \frac{E_a b_2}{t_a}\left(\frac{1}{E_1I_1}+\frac{1}{E_2I_2}\right)\sigma(x) + \frac{E_a b_2}{t_a}\left(\frac{y_1}{E_1I_1}-\frac{y_2}{E_2I_2}\right)\frac{d\ \tau(x)}{dx} + \frac{E_a 1}{t_a E_1 I_1}q = 0 \quad (2.43)$$

The general solution to this fourth-order differential equation is

$$\sigma(x)=e^{-\beta x}[C_1\cos(\beta x)+C_2\sin(\beta x)]+e^{\beta x}[C_3\cos(\beta x)+C_4\sin(\beta x)]-n_1\frac{d\tau(x)}{dx}-n_2q \quad (2.44)$$

For large values of x it is assumed that the normal stress approaches zero, and as a result $C_3=C_4=0$.

The general solution therefore becomes

$$\sigma(x)=e^{-\beta x}[C_1\cos(\beta x)+C_2\sin(\beta x)]-n_1\frac{d\tau(x)}{dx}-n_2q \quad (2.45)$$

Where

$$\beta = \sqrt[4]{\frac{E_a b_2}{4t_a}\left(\frac{1}{E_1I_1}+\frac{1}{E_2I_2}\right)} \quad (2.46)$$

$$n_1 = \left(\frac{y_1E_2I_2 - y_2E_1I_1}{E_1I_1+E_2I_2}\right) \quad (2.47)$$

and

$$n_2 = \frac{E_2 I_2}{b_2 (E_1 I_1 + E_2 I_2)} \tag{2.48}$$

In deriving *Equation (2.45)* it has been assumed that $d^5\tau/dx^5=0$, because $d^5\tau/dx^5$ generally has negligible significance to the final answer.

2.4 Analytical modelling of interfacial stresses

From the above equations we can arrive at the formulation for the theoretical values in the ideal case. For this calculation it was necessary to use MathCAD, a math-software that made the process of calculation easier and if once done it would be easy to reuse with minor changes. This MathCAD file was created by Dag Linghoff and is attached in the *Appendix A*. However minor changes were made to suit the particular test conditions given.

The shear stresses are calculated by using the formula according to Smith and Teng [5]

$$\lambda = \sqrt{\frac{G_{adh}.b_{CFRP}}{h_{adh}}\left[\frac{(y_1+y_2).(y_1+y_2+h_{adh})}{E_s.I_{el.no\_CFRP}+E_{CFRP}.I_{CFRP.el}}+\frac{1}{A_s.E_s}+\frac{1}{A_{CFRP}.E_{CFRP}}\right]} \tag{2.49}$$

$$m_2 = \frac{G_{adh}.y_1}{h_{adh}.E_s.I_{el.no\_CFRP}} \tag{2.50}$$

$$m_1 = \frac{G_{adh}}{h_{adh}.\lambda^2}\left(\frac{(y_1+y_2)}{E_s.I_{el.no\_CFRP}+E_{CFRP}.I_{CFRP.el}}\right) \tag{2.51}$$

$$k = \lambda.(b-a) \tag{2.52}$$

$$\tau_1(x_1) = \frac{m_2.P.a}{\lambda}.e^{-\lambda.x_1} + m_1.P - m_1.P.\cosh(\lambda.x_1).e^{-K} \tag{2.53}$$

2.5 Finite element modelling of adhesive joints

Types of Elements in ABAQUS

In finite element modelling there are many types of elements. The choice of the element depends on which set results the analysis is aimed at and how much computing power is available. Care should be taken as the choice of a wrong type of element could also give inaccurate results. Bogdanovich & Kizhakethara [1] in their paper talk about the three types of elements, which are:

- The first order (linear displacement) element or the 8-node hexadron.
- The second order (quadratic displacement) element or the 20-node serendipity hexadron.
- The 27 node full Lagrange hexadron element.

In the numerous works by the authors it was noted that the third type of element was the most accurate and computationally efficient. So they have worked with this type of element.

How ever Wu and Crocombe [2] have modelled Adhesive joints using three methods rather than elements.

- Simplified modelling- beam version.
- Two dimensional continuum modelling.
- Simplified modelling- hybrid version.

2.5.1 Simplified modelling - beam version

In this version the substrates are modelled by beam elements with the two connecting nodes of any element, and the adhesive will be modelled by plane four-node iso-parametric elements, the elements are not connected naturally so a rigid coupling relation is adopted to link the two kinds of connecting nodes. The displacements of a connecting node of the adhesive element are determined by those of a corresponding connecting node of the substrate element.

2.5.2 Two Dimensional Continuum Modelling

In the above-simplified modelling approach the effects of local deformations are ignored and the displacement compatibility is satisfied only at the connected nodes. To account for these the two dimensional continuum model is adopted where the adhesives are modelled in a similar way as the earlier method but the substrates are also modelled by four node iso-parametric elements in a compatible way.

2.5.3 Simplified Modelling – Hybrid version

This is basically a combination of the two above models. It was noted that the results of the above two methods matched except at locations of local deformation. So the adhesive is modelled in the same way as the above two methods but the substrates instead of using plane beam elements or four-node iso-parametric elements, a mixture of the two with the latter at the critical locations of local deformations is used. Thus the new model will have the simplicity of the earlier model and the accuracy of the second one. This way the hybrid method significantly reduces the computational effort.

2.5.4 The Sub-modelling concept

As we already know from the works of Wu and Crocombe [2] we can see that some parts of the joint model are critical so cannot be modelled by simple meshing. For example, the areas close to the lap ends in the case of a lap joint. Bogdanovich & Kizhakethara [1] suggests that these areas require more complex meshing like a non-uniform element mesh. The newer versions of ABAQUS® have a procedure called “sub-modelling”. This is a multi step procedure where the displacement and stresses for a successively reduced local region is calculated in several steps. The nodal displacement values in the previous step are applied as external boundary conditions for the next step so the new step should get a more accurate answer than the previous step.

2.6 A comparative study of ways to model an adhesive joint

Let us now compare and study different ways to model our problem in general. By ignoring the details and only considering the ways of modelling an adhesive joint, which is made of steel and CFRP as adherent and an epoxy as adhesive.

The whole exercise is aimed at finding out a method to model the three materials in ABAQUS and decide what sort of elements have to be used for the three materials.

Element selection has to be done carefully as complicated elements with more number of nodes would no doubt give an accurate result but it would also make the computation tedious and time taking and less efficient. If we could simplify those elements where required accuracy can be attained with just simple elements and hence reducing the over all computational effort required. So different people in this field have used many techniques to model this sort of a joint and here is a summary of some of them.

The first form of modelling in 3D is by the use of solid elements. The reason why this is not preferred is that the number of nodes is more making the amount of computational effort required extremely enormous. Besides as mentioned by Xinran Xio et al [6] solid element model for the adhesive would cause time step problems in dynamic analysis especially in LS DYNA.

So the two simplified models, which the author investigates, are described in the following sections

2.6.1 Tied (or) tie break contact

Here the surface-to-surface tiebreak contact is used. The tie break contact functions the same way as a common contact in compressive loads but under tension it allows the separation of the tied surface under a failure criteria like

$$\left(\frac{|\sigma_n|}{NFLS}\right)^2+\left(\frac{|\sigma_s|}{SFLS}\right)^2 \geq 1$$

Where NFLS is the normal failure stress and SFLS is the shear failure stress. This type of arrangement is shown in *Figure 2.2*

While using LS DYNA it is highly recommended to use tiebreak contact for adhesives and in ABAQUS the tied contact model is set up as tied node to surface contact (Tie break model is not allowed in ABAQUS Standard). ABAQUS XPLICIT allows separation of the bonded joint through bond command.

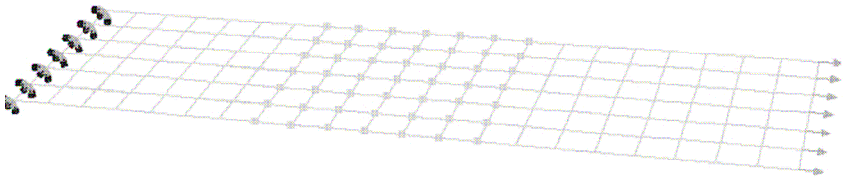

Figure 2.2 The tied-contact model for a DLS specimen. The adhesive bond is modelled as a tied contact between nodes and surface.

2.6.2 A line of rigid Links

It is defined as rigid links between the nodes of mating substrate pieces along a line across the width of the DLS specimen through the centre point of the overlap (*Figure 2.3)*. In ABAQUS the line of rigid links model uses rigid beam elements of RB2D2 as rigid links.

The authors concluded that for the substrates if modelled with shell elements and the adhesive with solid elements and rigid links between them to represent adhesive bonds result in a more compliant structural response. But using the contact definition in ABAQUS to represent the adhesive resulted in a much stiffer response as compared to the test results.

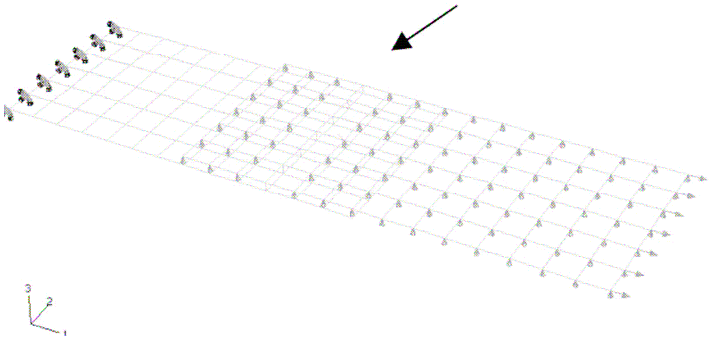

Figure 2.3 The line-rigid model for a double lap shear specimen. The adhesive bond is modelled as a line of rigid links (arrow).

Colombi & Poggi [7] also used the similar model with beam elements for adherents and 8-node plane stress elements for adhesive with rigid line links. The author also decreased the element size near the edges to account for local deformation due to stress concentration.

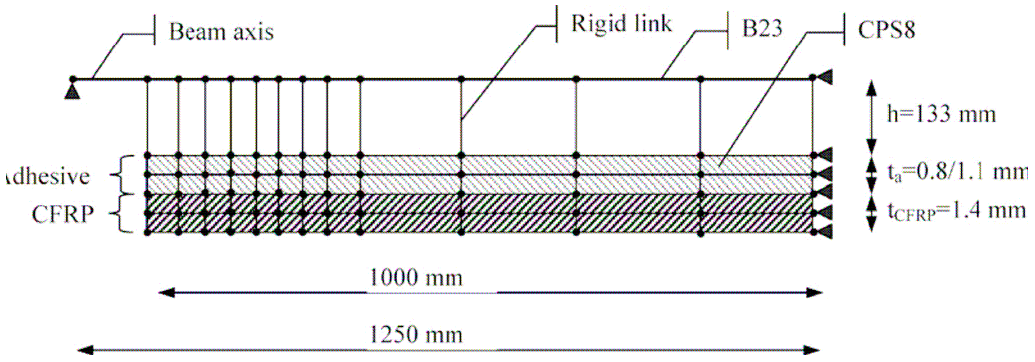

Figure 2.4 Modelling of the bonded reinforcement and necessary constraints to the steel beam.

Raul et al [11] has a different 2D-nonlinear adhesive formulation where adherents are modelled as Bernoulli/Euler beam elements with axial and bending deformation modes. The adhesive is a standard plane strain quadrilateral element except that the nodes are offset to coincide with the mid plane of the corresponding adherent the special adhesive element called ADH2D. This is shown in *Figure 2.5*

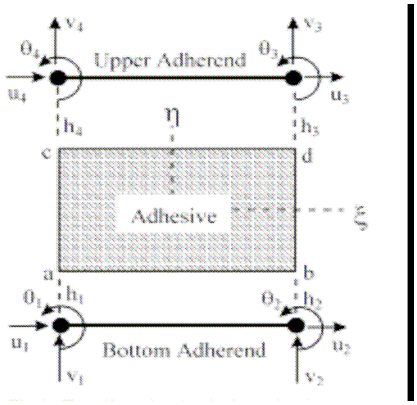

Figure 2.5 Two-dimensional adhesive finite elements.

A practical finite element approach has been developed at NASA Goddard Space Flight Centre to model the adhesive in a bonded joint. Numerical examples have shown good agreement with classical solutions.
According to Farhad [8] the method uses a gap with a thickness of the adhesive, two rigid elements, and three zero-length spring elements between coincident nodes. One rigid element stretches from one adherent to a node at the centre of the gap, while the second rigid element stretches from the other adherent to a coincident node also at the centre of the gap. The spring elements connect the two rigid elements between the coincident nodes. The *Figure 2.6* shows the layout. For clarity, the coincident nodes are shown separated. No rotational springs are used in this modelling technique.
Forces, stresses, strains, etc., can be recovered directly for the adherent elements. Recovery of spring forces and deformations can in turn be used to determine the stresses and strains in the adhesive.

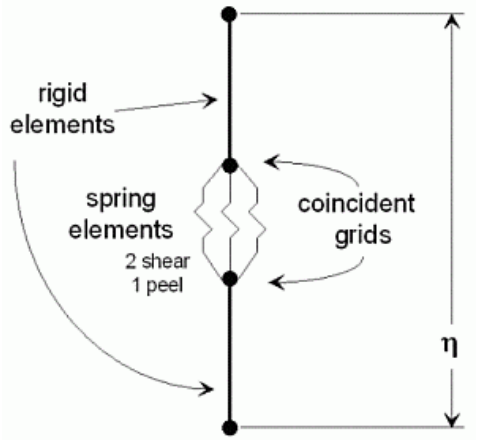

Figure 2.6 Farhad Tahmasebi's model with springs simulating the adhesive layer.

This model was interesting and seemed to have a logical method to calculate the interfacial stress components. Hence it was decided to use this model as a base in the present project and modify it to suit the present scenario.

3 Model and analysis method description

3.1 Modelling in ABAQUS

The process of modelling in ABAQUS was started early during the project immediately after the literature study but it only considered the basic features. The ABAQUS online reference manual [5] was a constant companion and proved to be an ocean of information.

The model consists of three physical parts and the rest of the conditions were applied as loads or boundary conditions. They are the steel beam, the CFRP laminate and the adhesive layer see *Figure 3.1*. Since it was decided to use spring elements to model the adhesive and its interfaces it is better to use two-dimensional shell elements both for the steel beam and the CFRP laminate.

To make the model time efficient the geometric symmetry of the beam in two directions were considered. To apply the symmetry only half of the beams both in the longitudinal and transverse directions are modelled and the boundary conditions applied in such a way so as to simulate the effect of the whole beam as shown in *Figure 3.2*

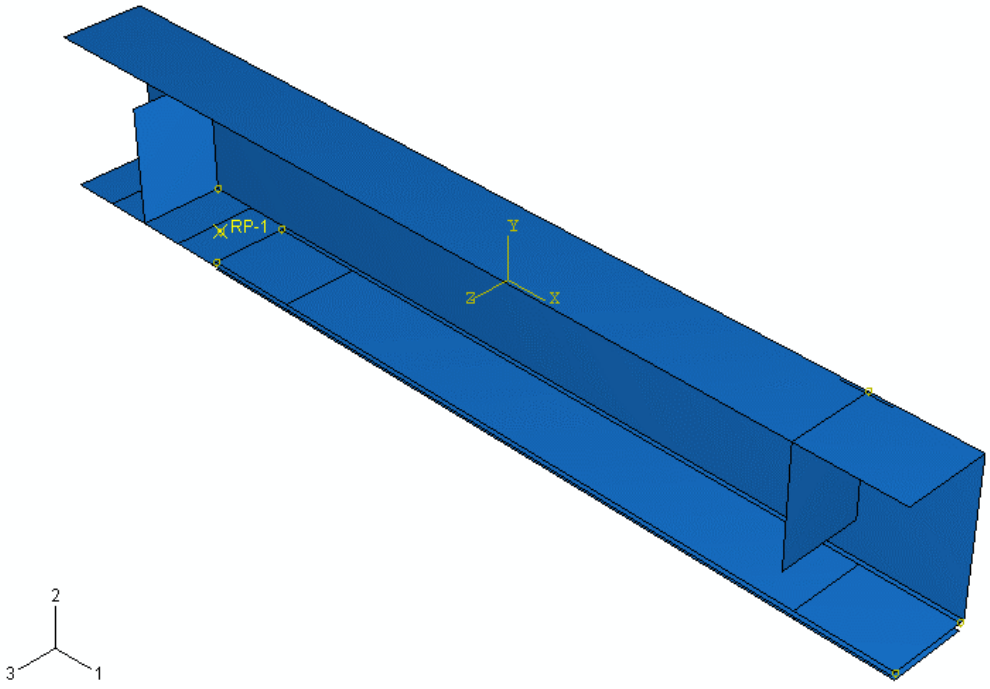

Figure 3.1 The model of the beam studied made in ABAQUS®.

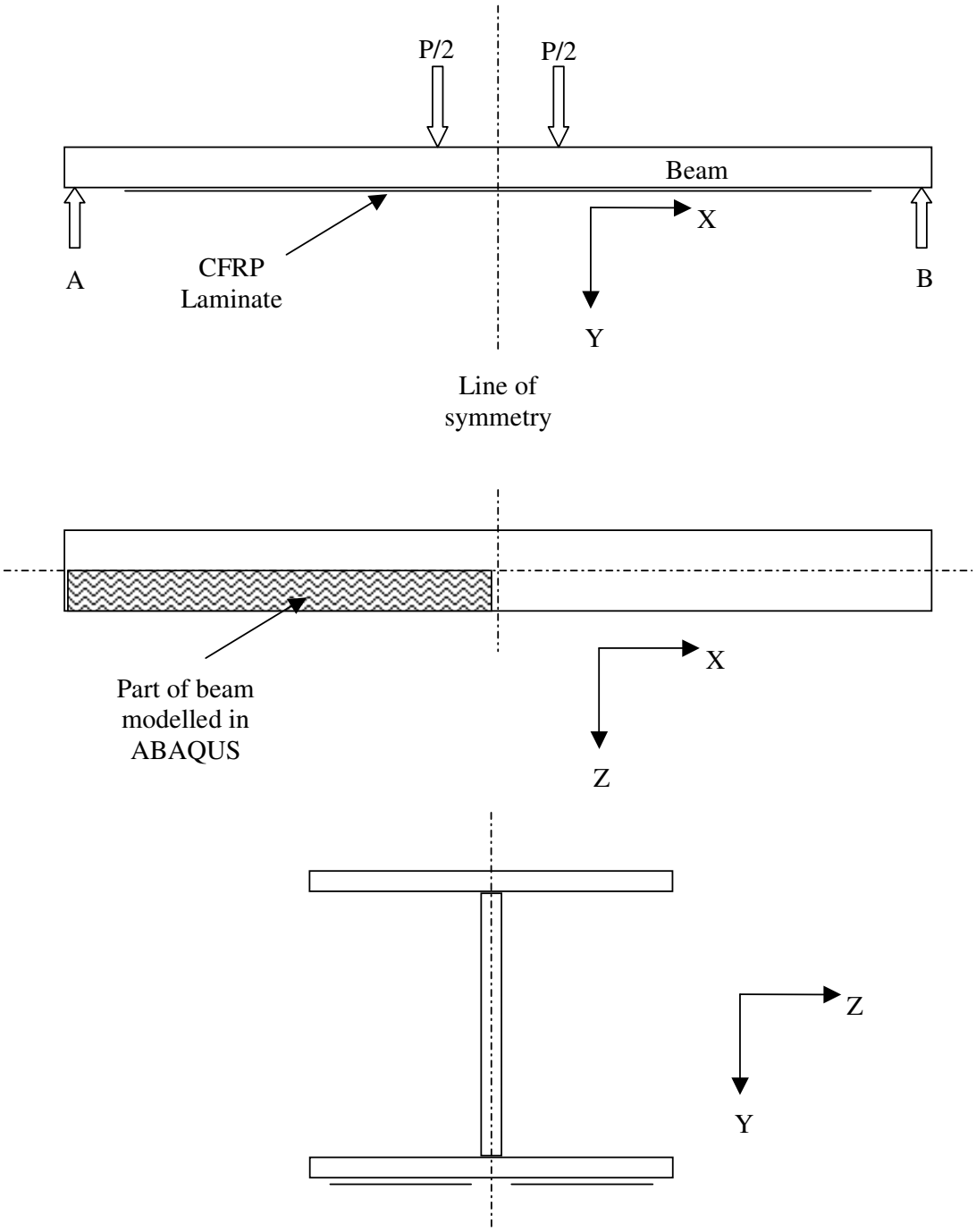

Figure 3.2 The Load application, symmetry, and boundary conditions.

3.1.1 Steel Beam

The steel beam was modelled with two-dimensional shell elements. The plates of different dimensions were first input as parts and then assembled by rotating and translating them into their place as if they were welded together. The flange plates were 9.5 mm thick and the web plate is actually 6 mm thick but due to symmetry it is set as only 3 mm. There are two stiffeners, each 10 mm thick as shown in the *Figure 3.1*

After the process of assembly, the whole beam is merged so that the parts don't act independent of each other. Necessary partitions for load application and meshing are also made and this is elaborated in the chapters that follow.

The material steel was modelled as elastic with a Young's modulus of elasticity of 212GPa and a Poisson's Ratio of 0.3 later on the material is upgraded to have a plastic property, which is dealt with in Chapter 6. The constitutive model used for steel is shown in *Figure 3.3*

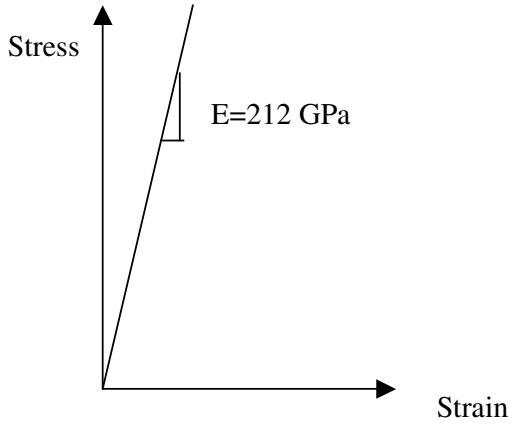

Figure 3.3 The Constitutive model for steel in the elastic state.

3.1.2 The CFRP laminate

Similar to the steel beam even the CFRP laminate is modelled with two-dimensional shell elements and is placed exactly below the beam with the spacing exactly enough to fit the adhesive layer in between the. The partitions on this laminate are made to facilitate meshing with different densities just as in the flange of the beam.

The material CFRP was modelled as elastic with a Young's Modulus of Elasticity of 200GPa and a Poisson's Ratio of 0.29 later on when the steel material was upgraded to have a plastic property the CFRP was assumed to be absolutely elastic which is dealt with in Chapter 6

3.2 Modelling of the interface

The interface was modelled using the spring connector elements and these connectors were given a property such that they represent the response of the adhesive layer.

An adhesive, which is not only a physical, layer it also shows interface properties of transferring shear and normal forces. Theses forces are transmitted either completely or partially depending on the capacity of the adhesive to transmit these forces.

The connector elements are the translation cartesian connectors CONN2D2 that stands for 2-dimensional 2-node connectors in ABAQUS.

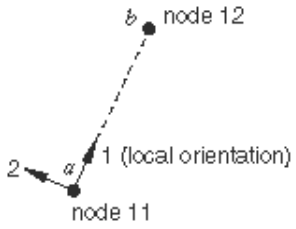

Figure 3.4 *The model of the spring connector used as taken from the ABAQUS documentation [9].*

These connectors can have three-dimensional action where they act along all the three major axes directions and have respective properties for each of them. The stresses in the third direction (along Z-axis) are not very dominant, so we can lock the displacement along this axis. Hence, the connector element that has been used has only 2-dimensional properties; they have a D11 and a D22. D11 as the name suggests is the relative elastic stiffness of the connector in that direction namely the X-axis direction and the D22 is the relative elastic stiffness of the connector in the 2-2 direction namely the Y-axis.

Relative elastic stiffness in a particular direction is the force (in the same direction) required to generate a unit displacement in that direction. Making use of this to simulate the behaviour of the adhesive, the force on the adhesive element to generate unit displacement can be calculated.

$$F = \sigma * A$$

$$Stiffness = \frac{F}{\delta}$$

$$F = \varepsilon * E * A$$

$$F = \frac{\delta}{l} * E * A$$

The stiffness an be defined as

$$\frac{F}{\delta} = \frac{EA}{l}$$

In case of single dimension (D22) use young's modulus of Elasticity and *l*=thickness of adhesive

$$\frac{F}{\delta} = \frac{GA}{l}$$

In case the spring replaces shear (D11) then G is used where G= Shear modulus of elasticity.

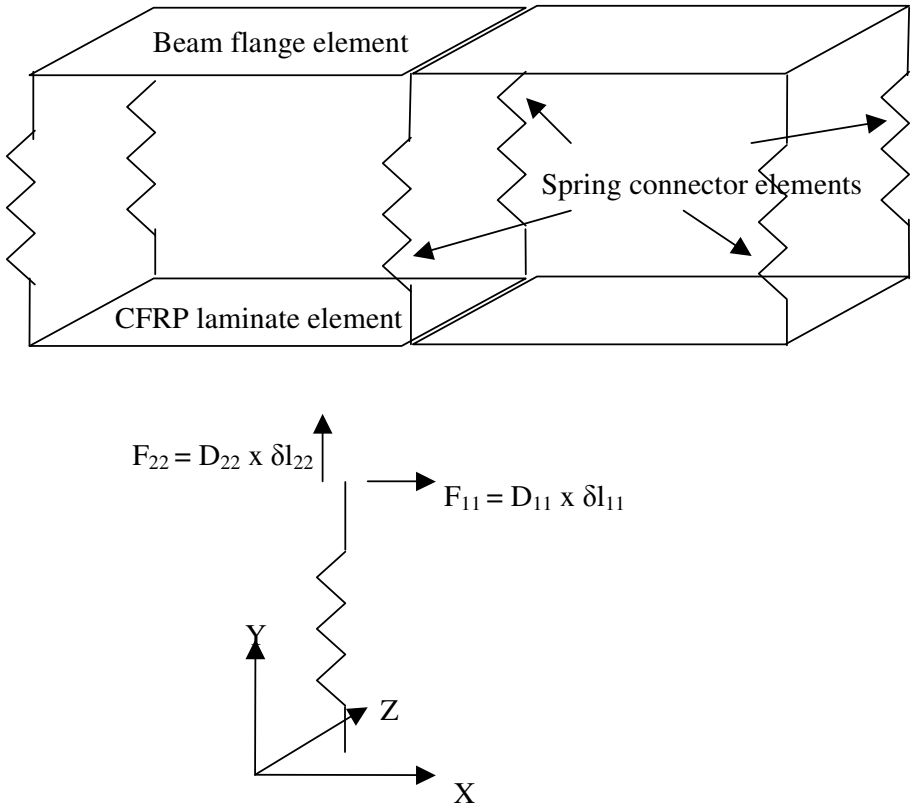

Figure 3.5 The analytical modelling of the adhesive with spring connectors.

To be able to place the connectors in the gap between the steel flange and the CFRP laminate it is necessary to have coincident nodes above and below so that we can have vertically connected nodes and the calculation is easy by avoiding the possibility of inclined springs.

This type of arrangement of the spring connectors gives us three types of springs for each mesh density where one single spring replaces one solid element cuboid of adhesive and thus has to replicate the effect of the force on this element cuboid. So the corner springs has to act as the cuboid of just one quarter the area of the element above and below it. Similarly for the springs on the edge it would have to act as the cuboid of half the area of the element above and below, and those away from the edges will act as the cuboid of cross sectional area equal to the area of the elements above and below.

The idea was to arrange these springs between two coincident meshes that would form an arrangement as shown in the *Figure 3.5* shown above. But this was not very easy in the present versions of ABAQUS®. The main reason being that each spring has to be placed manually and configured manually and with the highest mesh density tested it would be a colossal task to place *16441* spring connectors manually. So a method of placing the connectors had to be devised.

The suggestions for accomplishing this task were to place the spring connector into the input file by specifying the co-ordinates or re-numbering the nodes to make the coincident nodes have the same type of number and then follow a fresh user defined numbering pattern. But this proved difficult since the first method required heavy file operations using MATLAB and the latter was cumbersome and time consuming.

Instead of this, the node numbering in ABAQUS® was used to solve the problem of placing the spring connectors in place. Time was spent trying to study the numbering pattern that ABAQUS® follows and the mesh which was decided to be used was numbered in the same way both on the lower flange and the CFRP when they were meshed in a particular order.

The next task was to make a MATLAB code, which would follow this order and write the input code for ABAQUS® which when in turn was imported applied the spring connectors at coincident nodes. After successful completion of this part test drives were conducted to see it worked well and random checks were made to see the accurateness of the method.

How ever this method had one disadvantage that once there was any change in the meshing even a slight change it would make a whole new numbering pattern requiring the rewriting of the code to replicate the springs so care was taken not to disrupt it or change it as little as possible. This MATLAB code can be seen in *Appendix C*, and the part of the input generated by it will be the 9057 spring connectors and their locations.

3.3 Boundary conditions and load application

The beam was tested as a simply supported beam. To model it using symmetry, a support condition was applied to mimic the existence of the rest of the beam. This support condition allows rotation about the horizontal Z-axis and allows no other rotation or translation. On the line of the symmetry at the mid section for a simply supported beam the rotation about the Z-axis is locked and only the translation along the Y-axis is allowed.

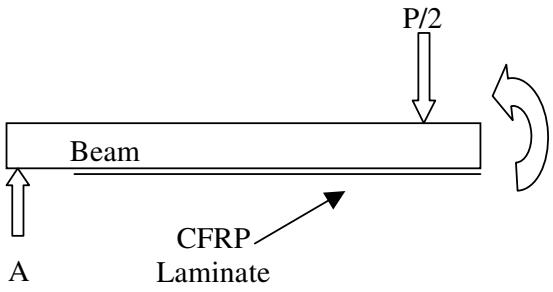

Figure 3.6 Boundary conditions of the beam model after making use of symmetry.

The longitudinal symmetry line which runs along the web of the beam reduces its thickness to 3 mm from 6 mm and to prevent it from lateral sway, the entire web is restricted from motion in the Z-direction.

The loads are applied as point loads on the top of the beam at the distance of *0.79m* from each support. But since in ABAQUS it's not possible to put point loads on shell elements, the loads are distributed over a length of *50 mm* and a breadth equal to the width of the web. Because of symmetry the load is divided into four to simulate the condition in the laboratory.

3.4 Meshing

Meshing is done in stages as a step-by-step development. Those regions of the composite beam that were found to be interesting were meshed again more finely after partitioning and seeding along the boundaries of those partitions.

First Meshing:

The first mesh used was coarse all over and had no partition except under the load since it was needed to demarcate the area of loading. But this mesh with 20 x 20 mm element size was not good enough to describe the shear along the length of the CFRP laminate.

Second Meshing:

During the second meshing the mesh size was reduced to 2mm square elements through out. But this gave rise to about 16441 nodes on the CFRP laminate and the density of the connectors connecting them was too high and it made the files very huge and the programme became time consuming. So this meshing was abandoned and the mesh density in the areas where the shear stress distribution was of less importance was decreased.

Third Meshing:

The CFRP laminate is partitioned into three parts with fine meshing (*2mmx2mm* elements) for the first *100 mm* on both sides along the length and in between a coarser mesh (*2mmx5mm* elements) is used.

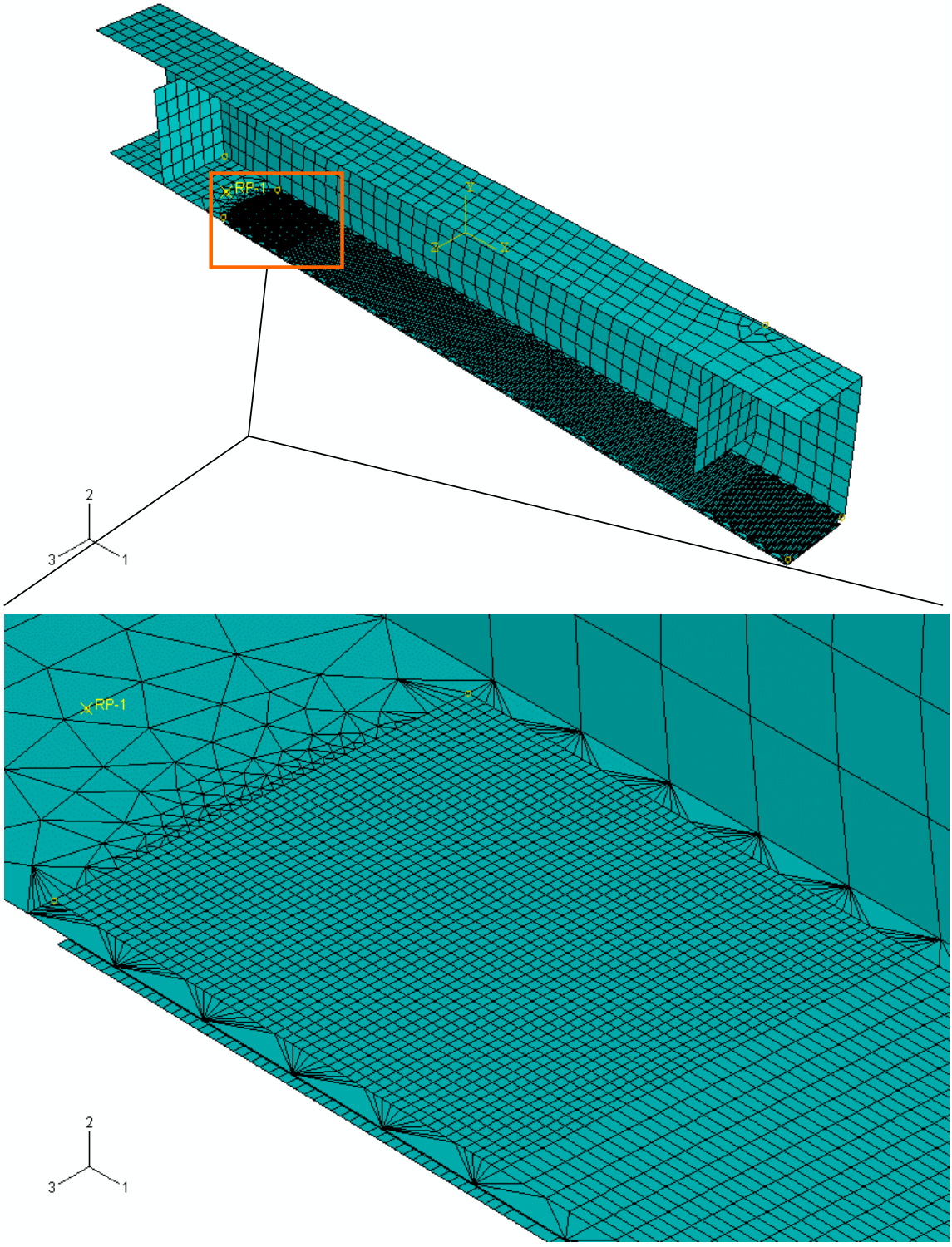

Figure 3.7 The mesh intensity illustrated on the lower flange.

4 Model Verification

To check the validity of the results and the accuracy of the model to deliver reasonable results it was necessary to compare it with an analytical solution or previously conducted tests and analysis. During such a comparison any variation in the results can be accepted if the reason for the variation can be explained.

4.1 Verification based on comparison with theoretical calculations

The deflection is calculated at the mid point of the beam with the CFRP bonded to the lower flange. These analytical results and the produced FE model should give the same deflection at the mid-section of the beam. To simplify the calculation of deflection for the purpose of model verification a load of 170 kN is chosen so that the section of the beams still is in elastic range

The deflection at mid point can be calculated as

$$Y_{mid} = \frac{2 * P * a_1 * (3 * L^2 - 4 * a_1^{\,2})}{48EI}$$

When P=load=85 KN.

a_1 =Distance to first load as in=0.79m

L=Length of beam=1.8m

EI=Young's modulus*moment of inertia= 5.E6 N.m^2

=4.042 mm

The midpoint deflection from the FE model gives a value of 4.5mm as can be seen from the graph in *Figure 4.1*

The deflection along the entire length of the beam was calculated using the MathCAD® file attached in *Appendix B*

The results are in good agreement as can be seen from the representation shown in *Figure 4.1*

There is a noticeable difference in the deflections of the FE models and the analytical solution because the analytical solution assumes that the elastic stiffness of the beam remains constant along the length of the beam while in reality for the first 100 mm from the support there is only the steel beam and no CFRP or adhesive and this is ignored and the analytical values are calculated assuming that the EI is constant along the entire length of the beam. Another reason for this for this behaviour can be the difference in the second moment off inertial. In the model with 2D shell elements there are no fillets while they are considered in the remaining cases and so the second moment of inertia of this model will be lower compared to the other two.

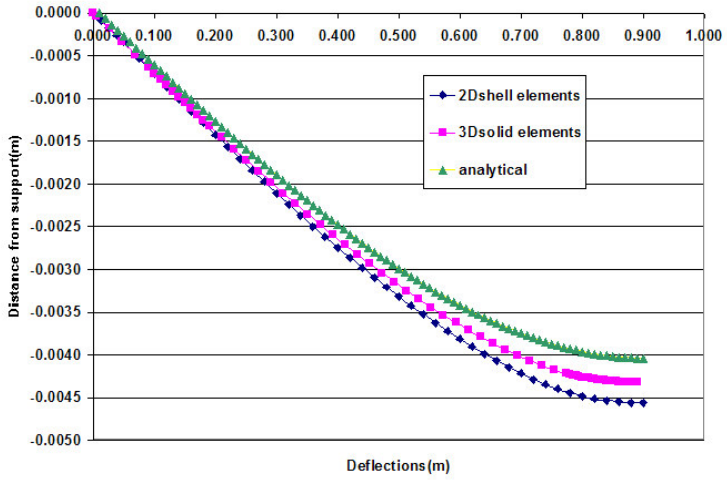

Figure 4.1 Comparison of Deflections along the length of the model.

4.2 Verification based on comparison with previous models

The tests carried out as a part of the Ph.D. research by Dag Linghoff was compared to the results from the FE analysis. The research consisted of both experiments in the laboratory and an FE model constructed was used and the results from them are studied in detail.

The model prepared by Dag Linghoff is similar to the one in this project except that it is modelled with three dimensional solid elements and it has a physical solid element adhesive layer. Also the fillets between the flanges and the web are also taken into consideration while they are ignored in this project.

In spite of the above differences a comparison between the deflections between the two results show very good agreement since the effect of these details on the total deflection are too minor to be noticed as can be seen in *Figure 4.1*.

Also studied was the comparison of the longitudinal normal stress distribution along the height of the beam at the mid section. As we can see from the *Figure 4.2*.

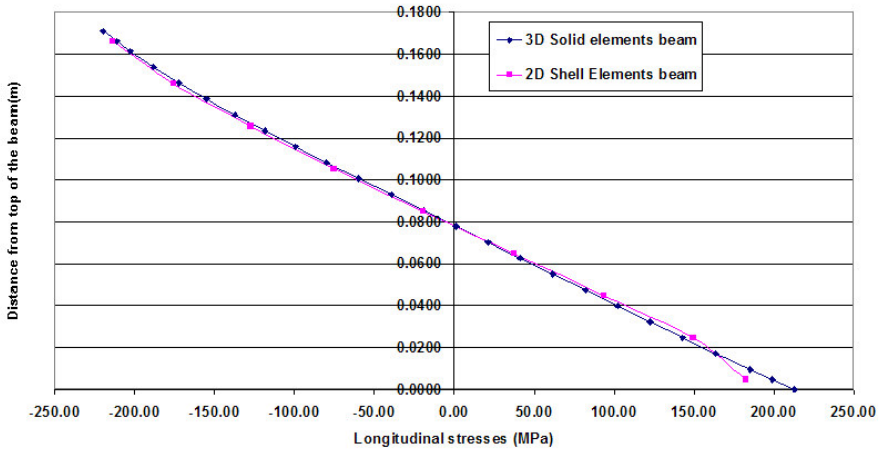

Figure 4.2 *Comparison of longitudinal normal stress distribution along the height of the beam at the middle section of the beam.*

It can be seen from this stress distribution the stresses are almost identical except at the lower flange where there is a small variation which can be explained by the difference in the type of modelling of the adhesive which contributes to the *EI* of the 3D solid element model but does not exists as a physical layer which in turn reduces the *EI* for the model with 2D shell elements and spring connectors for the adhesive.

The above two comparisons help us to arrive at the conclusion that the model is verified and can be used for further testing.

5 Analysis of interfacial stresses in the elastic phase

The analysis was run on the Chalmers UNICC (UNIX Numerical Intensive Computation at Chalmers) cluster of computers. The average runtime of the job is about 6 hours with a RAM utilization of 900 MB.

5.1 Comparison of shear stresses

Since the emphasis was on the interfacial stresses right from the beginning of the project and how these stresses change along the length and the breadth of the beam, let us now see how we can extract those values from the result files.

It was not possible to get the values of the shear stresses like in the model with 3D solid elements, as there was no such option given by ABAQUS, so these stresses had to be calculated by deriving the longitudinal normal stresses and the received shear stresses were plotted as shown in the *Figure 5.3*

The longitudinal normal stresses are taken from ABAQUS at every node on the line in consideration and then the difference between the stresses (longitudinal normal stresses) at each node and the node before it was taken and multiplied by the area of the region that the stress acts, then dividing it with the area between the two consecutive nodes would give us the mean shear stress between the two nodes in consideration. It is important that the order of calculating the difference be maintained along the entire line. For example in the *Figure 5.1* the difference if from the beginning was LS1-LS2 then it should be followed by LS2-LS3 in the next element.

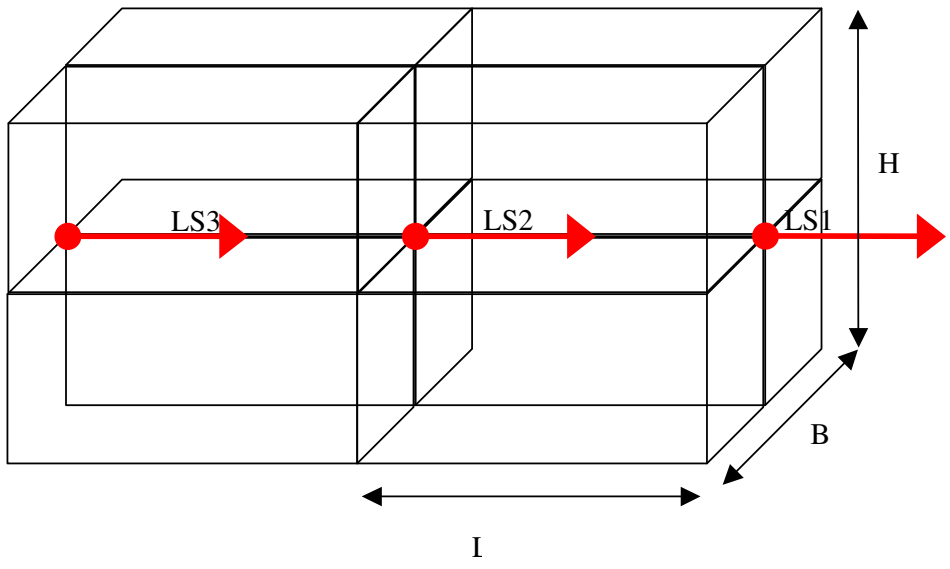

Figure 5.1 The derivation of longitudinal normal stresses to get shear stresses.

Difference in the longitudinal stresses at consecutive nodes is

= *LS1 - LS2*

Difference in forces is = *(LS1 - LS2) x B x H*

Shear stress is the difference in force/area

= *(LS1 - LS2) x ~~B~~ x H / L x ~~B~~*

Shear stress = *(LS1 - LS2) x H / L*

In comparison with these stresses are the analytical shear stresses obtained by the method described by Smith and Teng [5].

The comparison is made along three lines, which run along the length of the bond line. Their locations are chosen as close as possible to the inner edge, mid, outer edge of the adhesive layer as shown in the *Figure 5.2* below

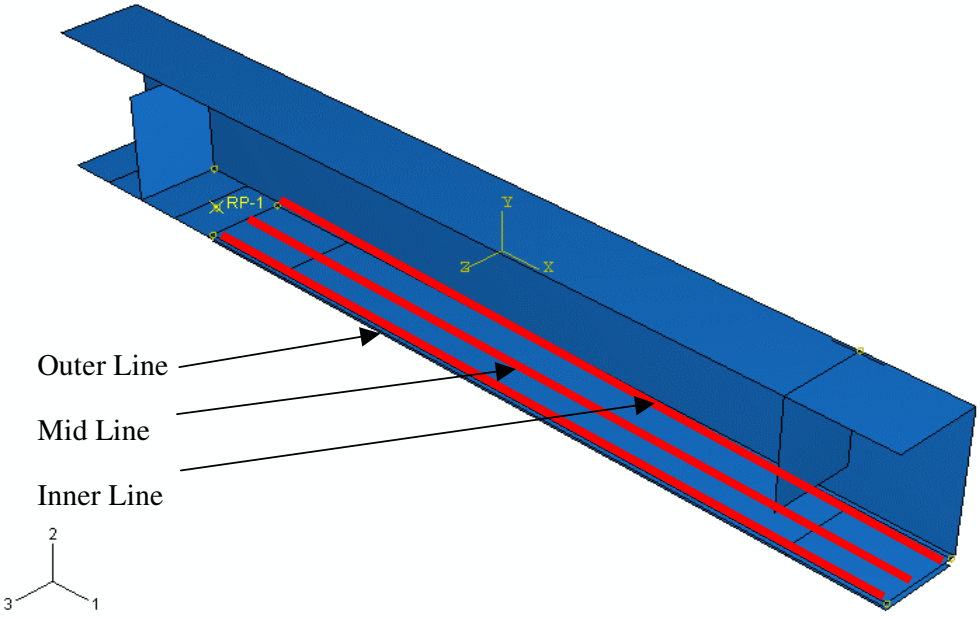

Figure 5.2 *The location of the three lines along which the shear stress distribution is studied.*

5.1.1 Shear stress distribution along the mid of the CFRP

The stresses are obtained from the centre of the CFRP strip along mid line to both the long edges of the laminate.

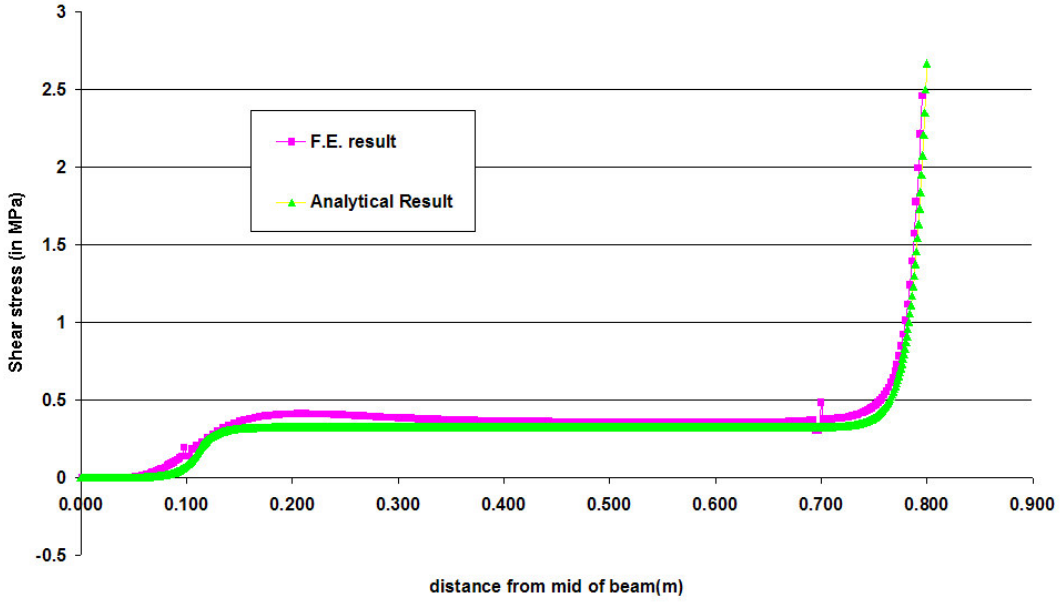

Figure 5.3 The shear stresses along the mid line of CFRP at 170kN.

The good agreement between the analytical and the FE results can be seen in the *Figure 5.3*. The differences in the FE result from model with 2D shell elements and the result from theoretical calculations are caused due to the following two reasons;

- The sudden abnormal disturbance situated exactly *100 mm* from the edges is caused due to the change in the mesh size. The spring connectors on this common border have only the properties of the smaller sized element. This creates a *1.5 mm* void in the adhesive layer which can be fixed by the use of the new properties which are calculated from the average properties of the two types of connectors on both sides.

- The slight variation of the shear stresses between the FE result and the theoretical results in the length of the beam between the load application points at the mid section of the beam can be explained. The theoretical calculation assumes that there is no shear stress acting between the load positions and in the FE analysis which is closer to the reality condition, there will be some shear stress between the CFRP and the beam due the curvature of the beam.

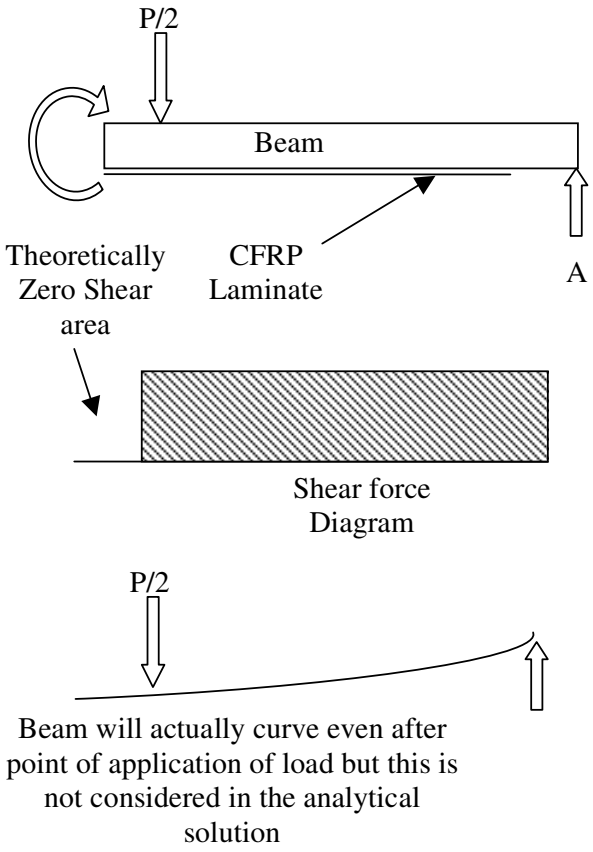

Figure 5.4 Effect of curvature on interfacial shear stress.

5.1.2 Shear stress distribution along the outer edge of the CFRP

Shear Stresses along the outer edge of the CFRP laminate is plotted in the similar way in *Figure 5.5* and then compared with the same analytical result as the shear stress distribution is assumed to be constant along the width of the laminate. Here too we notice that the shear stress curve from the 2D finite element model has a point every fixed interval, which has a value of shear stress equal to zero. This happens because the XY-data for the model in the form of distance (along X-axis) and longitudinal normal stresses are extracted from the ODB file, ABAQUS® allows an option where any missing value would be allowed to be interpolated for its value of x and some of these extra points are coincident points. During interpolation these coincident points have the same value as the previous point. If a graph showing the longitudinal stresses were to be plotted then it is not that visible in it since the adjacent points have the same value but when these stresses are derived, the difference in stresses between any interpolated value and its previous point is a zero and hence the shear stress at that point will be zero too. The real graph can be considered ignoring these abnormalities at fixed intervals as shown in *Figure 5.5*.

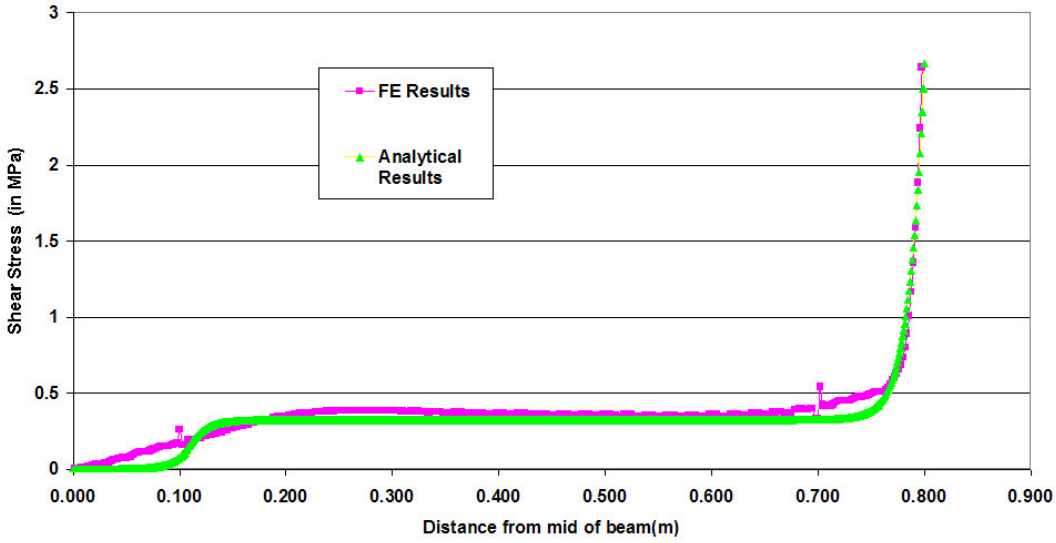

Figure 5.5 The shear stresses distribution along the outer edge of CFRP at 170kN.

5.1.3 Shear stress distribution along the inner edge of the CFRP

These stresses are obtained from the mid thickness of the CFRP strip along the inner edge of the laminate. Since these stresses come almost directly below the web they exhibit more extreme shear stresses variation from the analytical model given by Smith and Teng [5].

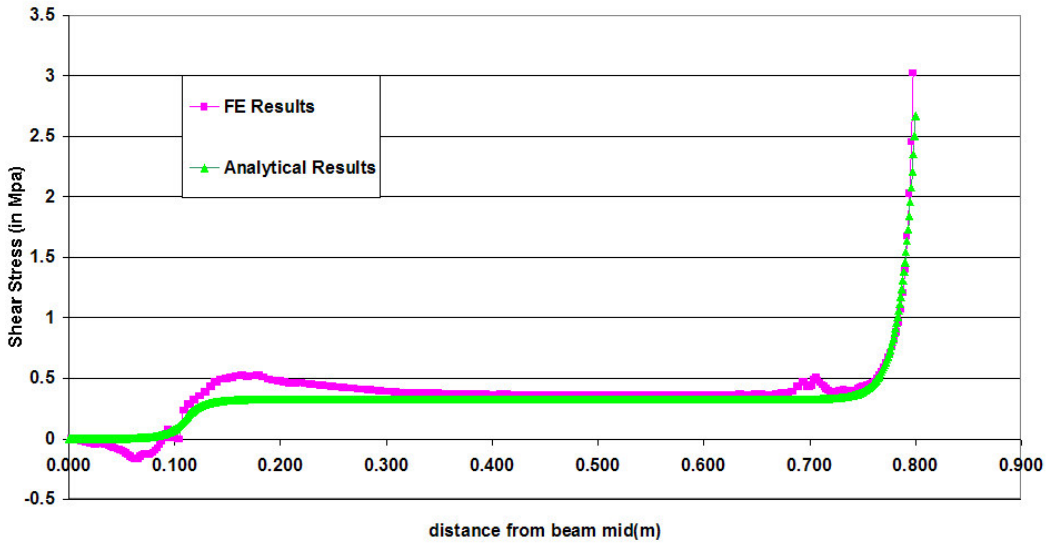

Figure 5.6 The shear stresses distribution along the inner edge of CFRP at 170kN.

5.2 Comparison of stresses across the width of the flange of the beam

The above comparisons only show the development of shear stresses along the three lines lengthwise. To get a better understanding of how shear stress varies along the width of the beam flange the shear stresses are plotted along a line at the edge of the laminate close to the support of the beam, see *Figure 5.7*. This is the location where there are maximum shear stresses (only in the elastic phase).

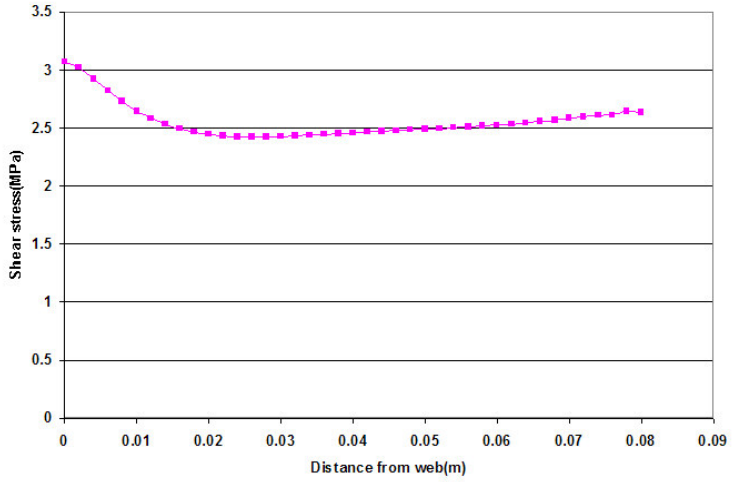

Figure 5.7 The shear stress distribution along the width of the flange.

5.3 Comparison of Normal stresses

The peeling stresses are also an important part of interfacial stresses. The 2D shell element FE model with spring connectors did not allow for the extraction of the Normal stresses directly since it wasn't possible to get the connector forces. But instead it was decided to get the difference in the displacements of the vertically coincident nodes and then by multiplying it with the stiffness of the spring connector we could arrive at the normal forces. But the difference in the displacement was so small in adjacent nodes that after 9 significant digits the difference in displacements ended getting rounded up giving abnormal rise and falls in the normal stress plot. Apart from this problem there is also another problem where though the nodes in the CFRP were made to coincide with the nodes on the lower flange, yet there was minor difference in the exact values of their coordinates, which generated additional points with null variables in the displacement extraction. Thus making the process of plotting almost manual and so it would be easier to not use this method for plotting the normal stresses.

6 Analysis of the interfacial stresses in the plastic phase

After the comparison of the results from the analysis done in the elastic state with the theoretical values the plastic properties of steel are input as material properties and the analysis run with the CFRP and the adhesive properties unchanged.

The elastic region of steel and the plastic stress strain relation based on the material tests conducted at CTH is input into the material properties. This relation is represented in *Figure 6.1*

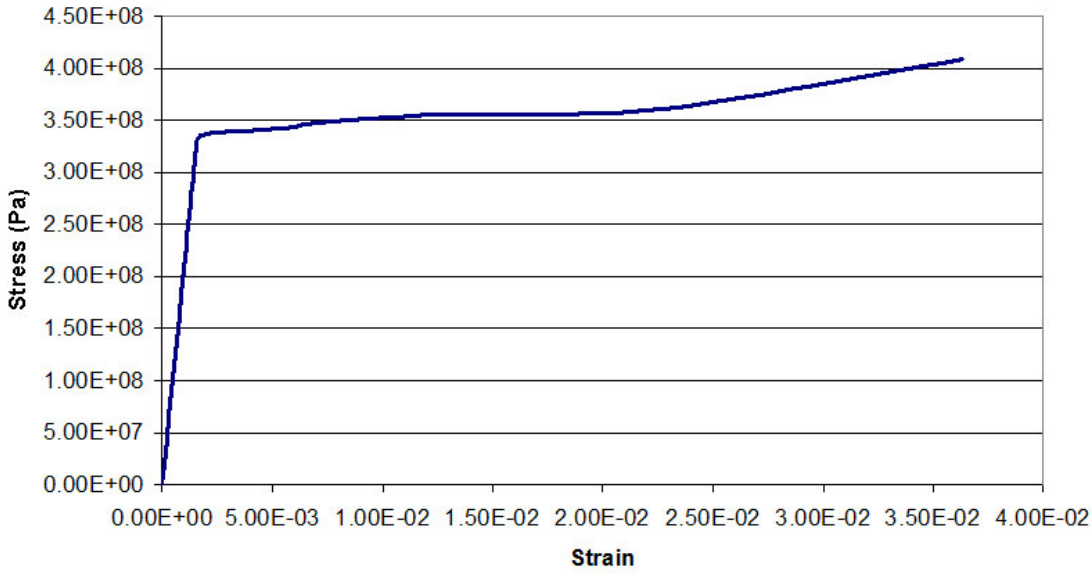

Figure 6.1 *The constitutive relation for both the linear elastic and non-linear plastic behaviour of steel.*

6.1 Comparison of shear stresses

The shear stresses along the length of the beam are compared in the same fashion as in the earlier chapter. Three lines, one near the inner edge, the second along the mid and third along the outer edge of the bond line between CFRP and the steel beam, are chosen to see how the shear stress changes along the length of the beam.

For the 2D shell element model the shear was calculated in the same way as described in *Section 5.1*.

Along with the series showing 2D shell elements model the older elastic analytical solution at 360kN is also plotted so that the shear in the interface when most of the beam is in the plastic state can be studied in comparison.

6.1.1 Shear stress distribution along a line through the middle of the CFRP

The stresses are obtained from the mid thickness of the CFRP strip along a line running mid way to both the edges of the laminate.

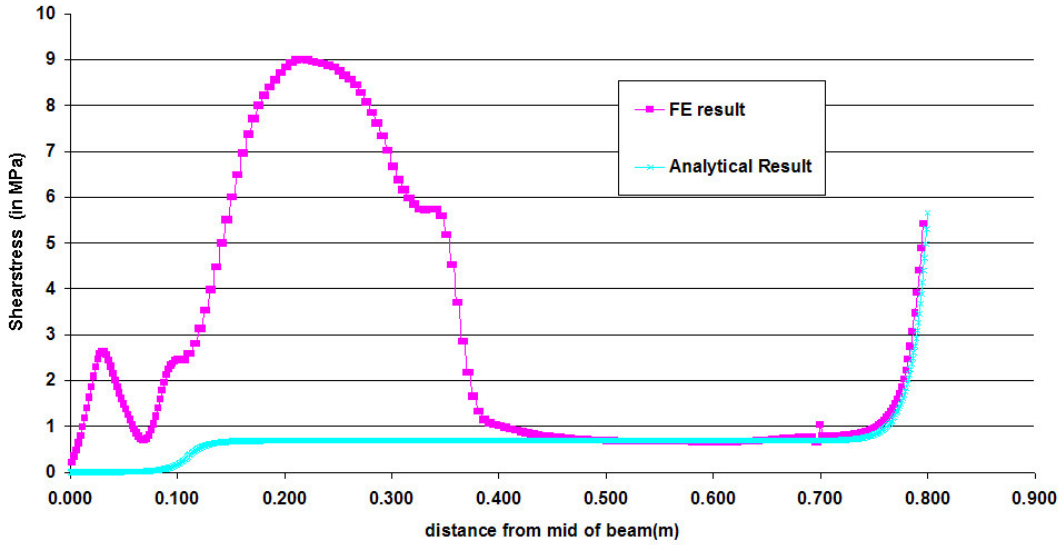

Figure 6.2 The shear stresses distribution along the mid line of CFRP at 360kN.

It can be seen from *Figure 6.2* that except in the plastic region where the beam is loaded, on the rest of the interface the shear stresses match the analytical results very well. So, for the non-plastic region that method is still valid and instead gives a safer solution too. These analytical results for the same beam are calculated for the load of 360kN using the same method as described earlier in *Section 2.4*

The disturbances in the smoothness in the FE result from model with 2D shell elements especially those situated exactly *100 mm* from the edges is caused due to the change in the mesh size the spring connectors on this common border have only the properties of the smaller sized element. This creates a *1.5 mm* void in the adhesive layer which can be fixed by the use of the new properties which are calculated from the average of properties of the type of connectors on both sides.

6.1.2 Shear stress distribution along the outer edge of the CFRP

Shear stresses along the outer edge of the CFRP laminate are plotted in the similar way. The results are then compared with the corresponding values from the analytical shear stress calculations.

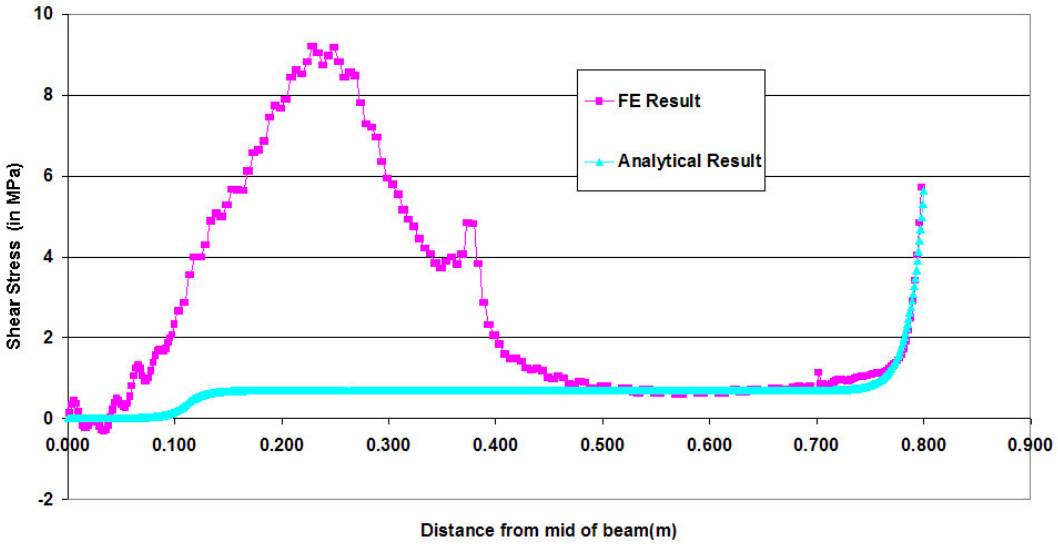

Figure 6.3 The shear stresses distribution along the outer edge of CFRP at 360kN.

We can see here the spring connector model shows shear stress very close to the analytical values away from the plastic region.

6.1.3 Shear stress distribution along the inner edge of the CFRP

These set of stresses are obtained from a line running along the inner edge of the bond line.

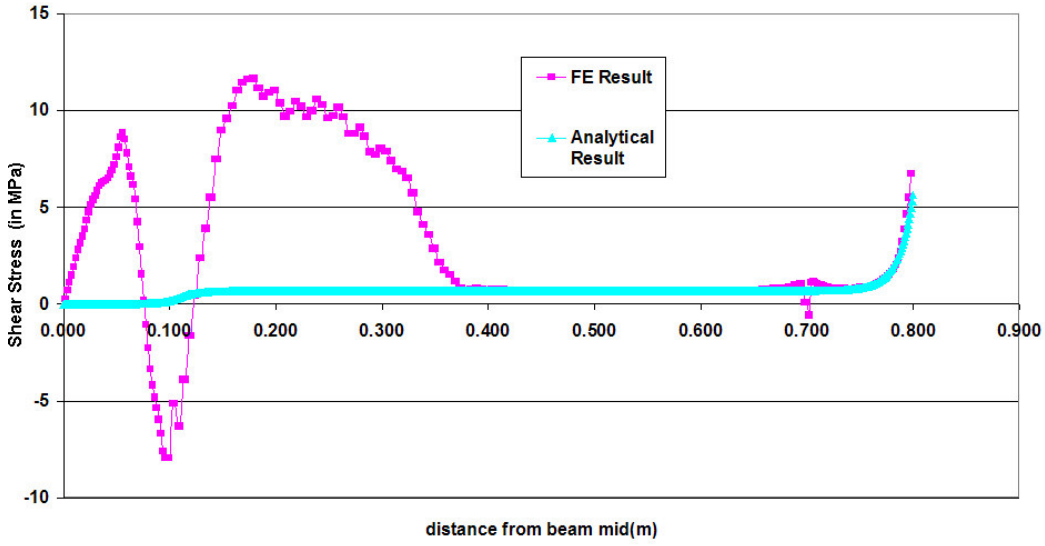

Figure 6.4 The shear stress distribution along the inner edge of CFRP at 360kN.

The *Figure 6.4* illustrates that the analytical stresses are valid for the region beyond the part where the beam is plastic and conservative too. In the laboratory tests there have been failures

occur near the support edge of the adhesive. Therefore the analytical solution is sufficient as it is very close to the real values for that region which is not yet plasticized.

6.1.4 Shear stress distribution across the width of the beam flange

The elastic analysis chapter it is necessary to see if in the plastic stage the shear stress distribution across the beam flange and it is found to have exactly the same pattern and shows little change except that it was higher due to increase in stresses. Shown in the *Figure 6.5* is this distribution along with the similar distribution at the elastic distribution of *170kN.*

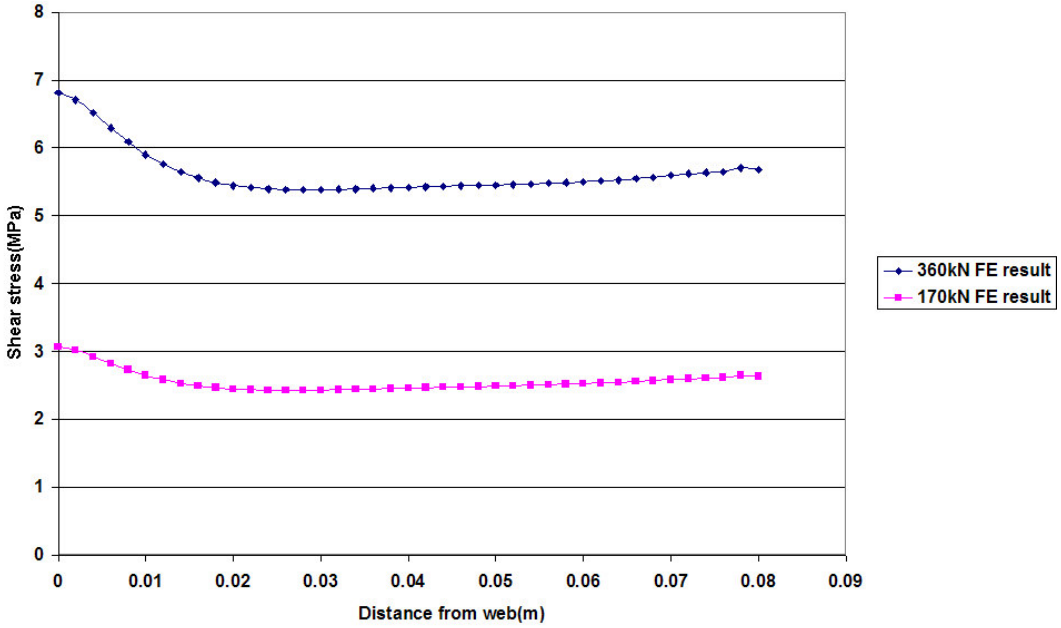

Figure 6.5 The shear stresses distribution along the width of the beam flange.

6.1.5 Shear stress development along the length of the bond line as load is increased

It would be interesting to study the effect of a step-by-step increase in the load and see how it affects the interfacial shear stresses. To achieve this, the loads when applied in ABAQUS® were done not at once, but in steps and each step was increased with small increments. Then after the analysis the following few important steps were chosen. These loads are 170kN for elastic, 270kN when yielding starts and then 292.5, 315 and 360kN for increasing degrees of plasticity of the beam.

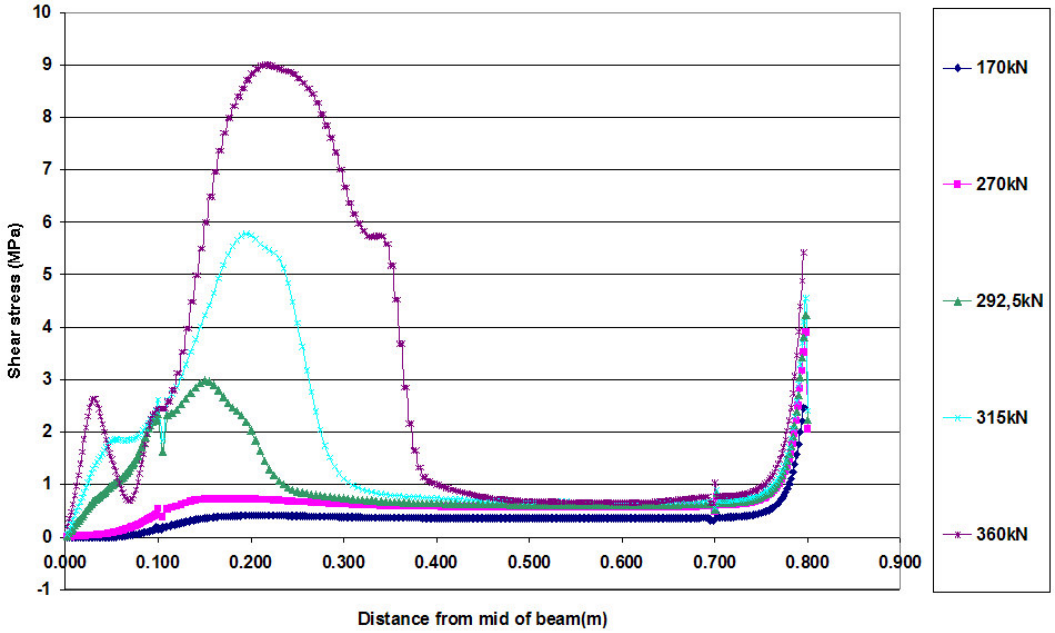

Figure 6.6 The shear stresses development along the length as load is increased stepwise.

The development clearly shows that the point of the beam with the highest shear stress clear moves towards the supports as the load on the beam increases (*Figure 6.6*). However on the shorter edge of the laminate the location of maximum shear does not change but the shear stress magnitude does increase. This increase can then be plotted as a shear stress against load-applied plot and it is shown in *Figure 6.7*.

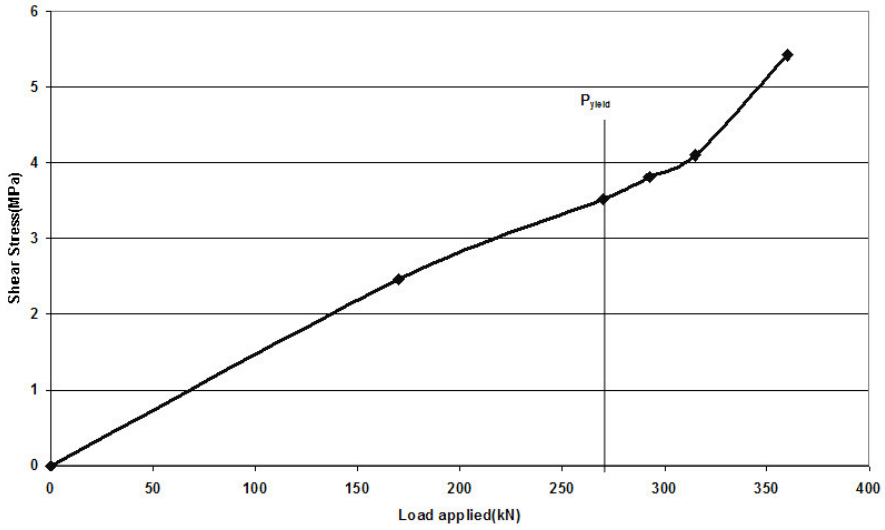

Figure 6.7 The shear stress at the edge of the laminate plotted against the applied load.

If the maximum shear stresses in the middle of the beam along the length are plotted it does not look like the *Figure 6.7* since those points do not occur at the same point as in the case of the stresses at the edge. A plot with the max shear stress development can be seen in *Figure 6.8*

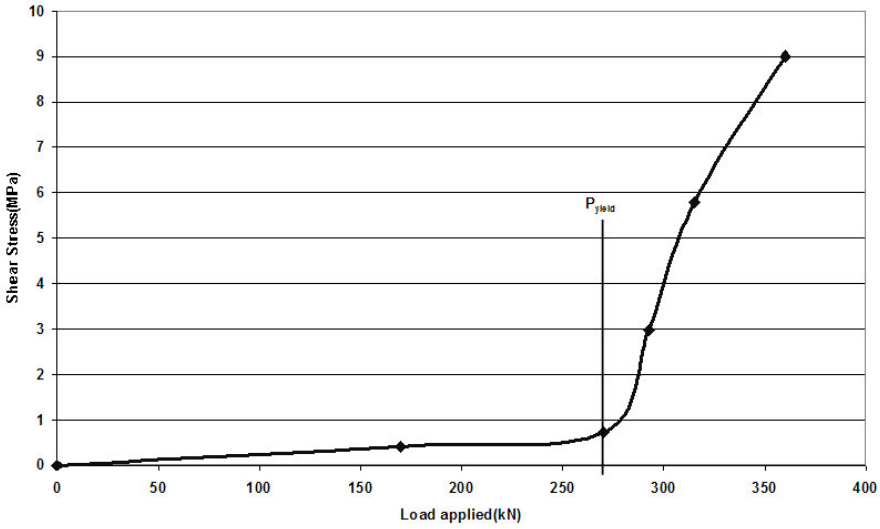

Figure 6.8 *The maximum shear stress in the middle of the beam plotted against the applied load.*

While referring to *Figure 6.8* it is good to remember that the points on the plot are not occurring at the same point and the points of maximum shear move towards the support, explaining the difference between the *Figure 6.7* and *Figure 6.8*

7 Conclusions and Recommendations

The results from the analysis with 3D solid elements and the 2D shell elements with the spring connectors proved to be satisfactory though the latter has a more laborious process for the result calculation.

7.1 Recommendations for further research

Some further research can be carried out since the results from this method of modelling the adhesive interface has been so close to the analytical results and especially if any better software can be used which can handle this sort of arranging of the springs and allow for working on a region of springs rather than each spring individually.

- Work could be done on using other software like ANSYS to do the same where modelling of that interface is much easier to handle.

- If three-dimensional solid elements are used instead of the 2D shell elements and the adhesives are modelled with spring connectors it would give an interesting result to study.

- May be it will be more advantageous to study current application where the CFRP is prestressed before being adhered to steel.

7.2 Final Conclusions

The development of the interfacial shear stress in the adhesive interface between CFRP and Steel in a composite beam modelled by the use of 2D shell elements and spring connectors for the adhesive interface was satisfactory. The following summarizes the conclusion of this thesis work.

- The interfacial shear stresses calculated from this result is in excellent agreement with the theoretical values.

- The process of making an array of springs was easy in this case but will get extremely complicated in the case of three dimensional shape of adhesive layer.

- The extraction of normal forces from the difference in the displacement should not be tried for small-scale models where displacements are very low since the values, which get rounded of, will affect these and therefore a better method should be followed for it.

- Plastic analysis shows that except under the load where the shear stresses are too high where the failure occurs (i.e. near the support edge of the CFRP) the stresses calculated by the conventional theoretical methods are still valid and in fact on the safer side (conservative).

8 Reference

1 Three dimensional finite element Analysis of double lap composite adhesive bonded joint using submodeling approach (1999) By A.E. Bogdanovich & I. Kizhakethara

2 Simplified finite Element Modelling of structural Adhesive Joints (1994) By Gaofeng Wu & A. D. Crocombe

3 Technical Report, Sustainable Bridges (2004) By Otto Norling, Sto Scandinavia AB

4 Mechanics of Composite Structural Elements (2004) By H.Altenbach, J.Altenbach & W.Kissing Ref No: ISBN 3-540-40865-7

5 Interfacial Stresses in plated beams (2000) By S.T. Smith and J.G. Teng

6 Stiffness prediction of the double lap shear joint, Part II: Finite Element Modelling (2003) By Xinran (Sharon) Xiao, Peter H Foss, and Jessica A Schroeder.

7 An Experimental, Analytical and numerical study of the static behaviour of steel beams reinforced by pultruded CFRP strips (2004) By Pierluigi Colombi, Carlo Poggi.

8 Finite Element Modelling of an Adhesive in a bonded joint (1999), By Farhad Tahmasebi, PhD, NASA, Goddard Space Flight Centre

9 ABAQUS 6.4.1 Reference manual (online version)

10 A three Dimensional Finite Element Model for stress analysis of adhesive joints (2002) by J.P.M. Goncalves, M.F.S.F. de Moura, P.M.S.T. de Castro

11 Two and three dimensional geometric Non linear finite element for analysis of adhesive joints. (2000) By Raul H Andruet, David A. Dillard, Siegfried M Holzer.

Appendix A

Analysis of the I-section with two point loads 170kN

MathCAD file that calculates the interfacial Shear stress according to Smith and Teng [5]

Analysis of an I-Section: Point load

This program calculates moment and the interfacial shear and normal stresses, in the elastic phase

Annotation:

b=beam, s=steel, CFRP=CFRP, adh=adhesive, y=yield, el=elastic, pl=plastic, ue=upper edge, le=lower edge

$MPa := 10e6 \cdot Pa$

$GPa := 10e9 \cdot Pa$

$kN := 1000N$

$kNm := 1kN \cdot m$

Beam (Steel):

HEA 180

$\sigma_{y.s} := 328 \cdot MPa$

$E_s := 212GPa$

$v_s := 0.3$

$h_w := 152mm$

$t_w := 6.0mm$

$L_b := 1.8 \cdot m$

$d_s := 7800 \cdot \frac{kg}{m^3}$

$b_{fl} := 180mm$

$t_{fl} := 9.5mm$

$G_s := \frac{E_s}{2 \cdot (1 + v_s)}$

$G_s = 1.995\times 10^{4}\ \text{Pa}$

$R := 15\cdot 10^{-3}\,\text{m}$

$h_b := h_w + 2t_{fl}$

$h_b = 0.171\,\text{m}$

$\varepsilon_{y.s} := \frac{\sigma_{y.s}}{E_s}$

$\varepsilon_{y.s} = 1.031$

$A_{R\_tot} := (2\cdot R)^2 - \pi\cdot R^2$

$A_s := 2\cdot\left(b_{fl}\cdot t_{fl}\right) + h_w\cdot t_w + A_{R\_tot}$

$A_s = 4.525\times 10^{-3}\ \text{m}^2$

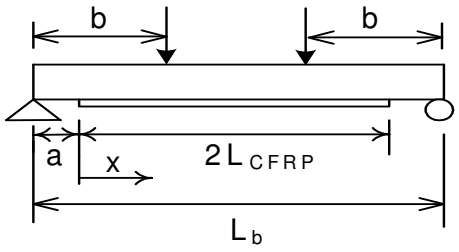

$A_w := h_w\cdot t_w$

$A_{fl} := t_{fl}\cdot b_{fl}$

$a := 0.10\,\text{m}$

$b := 0.790\,\text{m}$

Composite material

$\sigma_{y.CFRP} := 3100\,\text{MPa}$

$E_{CFRP} := 200\,\text{GPa}$

$h_{CFRP} := 0.0014\,\text{m}$

$b_{CFRP} := 0.120\,\text{m}$

$v_{CFRP} := 0.3$

$d_{CFRP} := 1600 \frac{kg}{m^3}$

$G_{CFRP} := \frac{E_{CFRP}}{2 \cdot (1 + v_{CFRP})}$

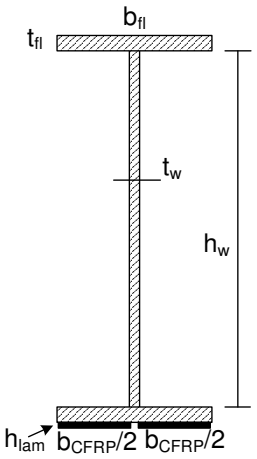

$G_{CFRP} = 1.882 \times 10^{4}\ Pa$

$I_{CFRP.el} := \frac{b_{CFRP} \cdot h_{CFRP}^{3}}{12}$

$\varepsilon_{y.CFRP} := \frac{\sigma_{y.CFRP}}{E_{CFRP}}$

$\varepsilon_{y.CFRP} = 10.333$

$A_{CFRP} := b_{CFRP} \cdot h_{CFRP}$

$A_{CFRP} = 1.68 \times 10^{-4}\ m^2$

Adhesive material

$E_{adh} := 7 \cdot GPa$

$h_{adh} := 0.002 m$

$v_{adh} := 0.3$

$\tau_{adh.max} := 25 \cdot MPa$

$$G_{adh} := \frac{E_{adh}}{2\cdot(1 + v_{adh})}$$

$G_{adh} = 658.661\text{Pa}$

STEP I: Elastic state

Distance between upper edge and the center of gravity.

$$y_{CG} := \frac{\left[t_{fl}\cdot b_{fl}\cdot\left(t_{fl} + 3\cdot\frac{t_{fl}}{2} + h_w\right) + h_w\cdot t_w\cdot\left(t_{fl} + \frac{h_w}{2}\right)\right]\cdot d_s + h_{CFRP}\, b_{CFRP}\cdot\left(2\cdot t_{fl} + h_w + \frac{h_{CFRP}}{2}\right)\cdot d_{CFRP}}{A_s\cdot d_s + A_{CFRP}\, d_{CFRP}}$$

$y_{CG} = 0.0843\text{m}$

Distance from the top of the upper flange to the centre of gravity.

$y_{CG.bott} := 2\cdot t_{fl} + h_w + h_{CFRP} - y_{CC}$

Distance from the bottom of the CFRP to the centre of gravity.

Distance between upper edge and the neutral axis

$$y_{NA} := \frac{\left[t_{fl}\cdot b_{fl}\cdot\left(t_{fl} + 3\cdot\frac{t_{fl}}{2} + h_w\right) + h_w\cdot t_w\cdot\left(t_{fl} + \frac{h_w}{2}\right)\right] + h_{CFRP}\, b_{CFRP}\cdot\left(2\cdot t_{fl} + h_w + \frac{h_{CFRP}}{2}\right)}{A_s + A_{CFRP}}$$

$y_{NA} = 0.087\,\text{m}$

Distance from the top of the upper flange to the neutral axis (NA) of the cross-section

$y_{NA.bott} := 2\cdot t_{fl} + h_w + h_{CFRP} - y_{NA}$

$y_{NA.bott} = 0.086\text{m}$

Distance from the bottom of the CFRP to the neutral axis (NA).

Cross-sectional constants, for the beam without CFRP

$$I_{el.no\_CFRP} := 2\cdot\left[b_{fl}\cdot\frac{t_{fl}^3}{12} + A_{fl}\cdot\left(\frac{h_w}{2} + \frac{t_{fl}}{2}\right)^2\right] + t_w\cdot\frac{h_w^3}{12}$$

Moment of inertia

$I_{el.no\_CFRP} = 2.408\times 10^{-5}\ \text{m}^4$

$$W_{el.no\_CFRP} := \frac{2I_{el.no\_CFRP}}{h_b}$$

$W_{el.no\_CFRP} = 0.282\,L$

Maximum elastic moment and point load, for the beam without CFRP

$M_{el.no\_CFRP} := \sigma_{y.s} \cdot W_{el.no\_CFRP}$

$M_{el.no\_CFRP} = 15.068\,N \cdot m$

$P_{el.no\_CFRP} := \frac{M_{el.no\_CFRP}}{b}$

$P_{el.no\_CFRP} = 0.019\,m\frac{kN}{m}$

Cross-sectional constants, for the beam with CFRP

$$I_{el.CFRP} := b_{fl} \cdot \frac{t_{fl}^3}{12} + A_{fl} \cdot \left(y_{NA} - \frac{t_{fl}}{2}\right)^2 + t_w \cdot \frac{h_w^3}{12} + A_w \cdot \left[y_{NA} - \left(t_{fl} + \frac{h_w}{2}\right)\right]^2 \ldots$$
$$+ b_{fl} \cdot \frac{t_{fl}^3}{12} + A_{fl} \cdot \left(y_{NA.bott} - h_{CFRP} - \frac{t_{fl}}{2}\right)^2 + \frac{E_{CFRP}}{E_s} \cdot \left[b_{CFRP} \cdot \frac{h_{CFRP}^3}{12} + A_{CFRP}\left(y_{NA.bott} - \frac{h_{CFRP}}{2}\right)^2\right]$$

$I_{el.CFRP} = 2.523 \times 10^{-5}\,m^4$

$W_{el.CFRP} := \frac{I_{el.CFRP}}{y_{NA}}$

$W_{el.CFRP} = 0.291\,L$

Maximum elastic moment and point load, for the beam with CFRP

$M_{el.CFRP} := \sigma_{y.s} \cdot W_{el.CFRP}$

$M_{el.CFRP} = 15.551\,N \cdot m$

$P_{el.CFRP} := \frac{M_{el.CFRP}}{b}$

$P_{el.CFRP} = 0.02\,kN$

Calculation of strain and stress over the cross-section for a specific load (Elastic):

<u>No CFRP:</u>

Applied load:

$P_1 := \frac{170}{2} \cdot kN$

(Total load/number of loadpoints)

$M_s := P_1 \cdot b$

$M_s = 67.15\,kNm$

$$\sigma_s := \frac{M_s}{W_{el.no\_CFRP}}$$

$\sigma_s = 1.462 \times 10^6\,MPa$

$$\varepsilon_s := \frac{\sigma_s}{E_s}$$

$\varepsilon_s = 4.597 \times 10^3$

$$\frac{\varepsilon_s}{1.05 \cdot 10^{-3}} = 4.378 \times 10^6$$

Analytical strain compared with result from FEM.

Moment and straindistribution over a length x_s for the apllied load P_1:

$x_s := 0m, 0.01m .. b$

$M_{sd}(x_s) := P_1 \cdot x_s$

$$\sigma_{sd}(x_s) := \frac{M_{sd}(x_s)}{W_{el.no\_CFRP}}$$

$$\varepsilon_{sd}(x_s) := \frac{\sigma_{sd}(x_s)}{E_s}$$

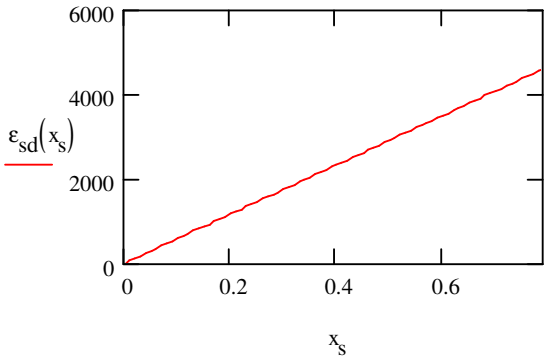

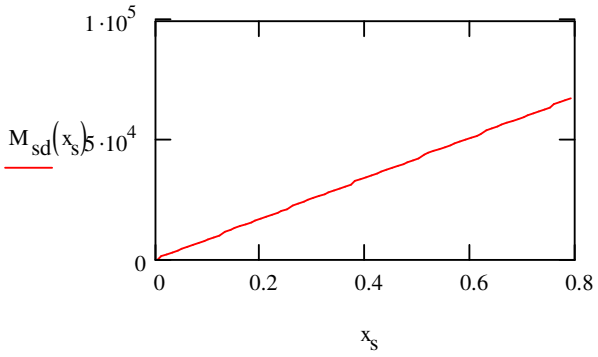

Calculation of shear stress and normal (peeling) stress in the elastic phase: (S.T. Smith and J.G. Teng)

This solution describes the stresses in the adhesives at the end of the CFRP. The solution for the shear stress is only valid for two symmetrically positioned point loads, while the solution concerning normal stress is valid for both uniformly distributed loads and point loads.

$$P := \frac{170}{2}\,kN$$

$P = 85\,kN$

$b = 0.79\,m$

$x_1 := 0m, 0.001m .. 0.690m$

$x_2 := 0.691m, 0.692m .. 0.80m$

Shear stress:

$$y_1 := \frac{h_w}{2}$$

$$y_2 := \frac{h_{CFRP}}{2}$$

$$\lambda := \sqrt{\frac{G_{adh}\cdot b_{CFRP}}{h_{adh}}\cdot\left[\frac{(y_1+y_2)\cdot(y_1+y_2+h_{adh})}{E_s\cdot I_{el.no\_CFRP}+E_{CFRP}\cdot I_{CFRP.el}}+\frac{1}{A_s\cdot E_s}+\frac{1}{A_{CFRP}E_{CFRP}}\right]}$$

$$m_2 := \frac{G_{adh}\cdot y_1}{h_{adh}\cdot E_s\cdot I_{el.no\_CFRP}}$$

$$m_1 := \frac{G_{adh}}{h_{adh}\cdot\lambda^2}\cdot\left(\frac{y_1+y_2}{E_s\cdot I_{el.no\_CFRP}+E_{CFRP}\cdot I_{CFRP.el}}\right)$$

$$k := \lambda\cdot(b-a)$$

$$\tau_1(x_1) := \frac{m_2 \cdot P \cdot a}{\lambda} \cdot e^{-\lambda \cdot x_1} + m_1 \cdot P - m_1 \cdot P \cdot \cosh(\lambda \cdot x_1) \cdot e^{-k}$$

$\tau_{max} := \tau_1(0mm)$

$\tau_{max} = 1.657 \times 10^4 MPa$

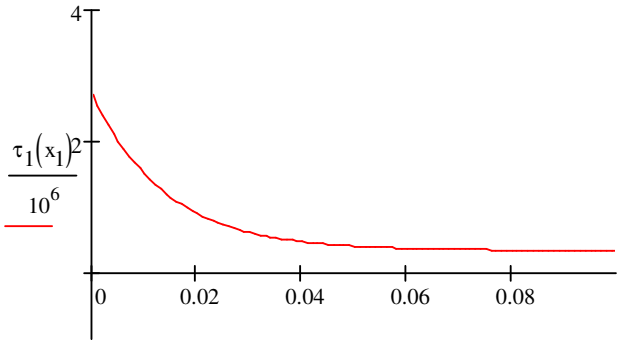

$$\tau_2(x_2) := \frac{m_2 \cdot P \cdot a}{\lambda} \cdot e^{-\lambda \cdot x_2} + m_1 \cdot P \cdot \sinh(k) \cdot e^{-\lambda \cdot x_2}$$

$\tau_{max} := \tau_2(0.79lm)$

$\tau_{max} = 0.717MPa$

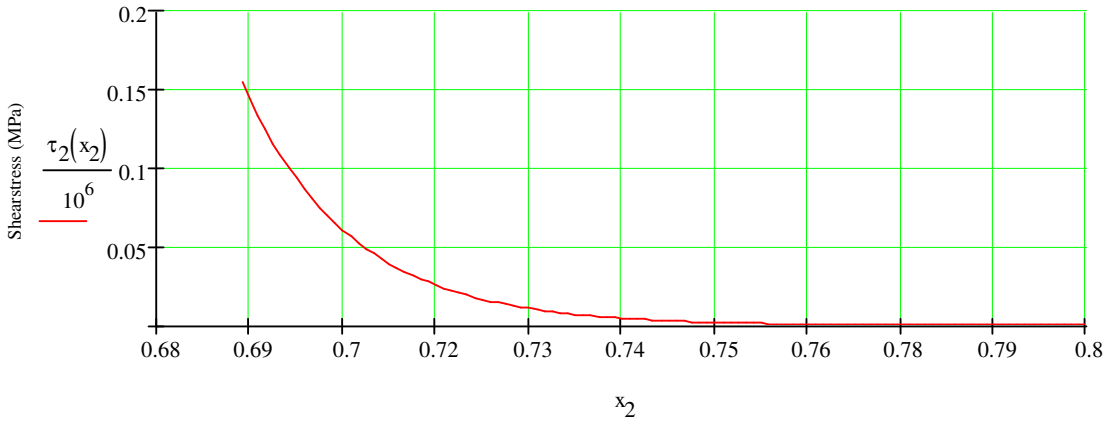

Normal stress:

$$n_1 := \frac{y_1 \cdot E_{CFRP} \cdot I_{CFRP.el} - y_2 \cdot E_s \cdot I_{el.no\_CFRP}}{E_s \cdot I_{el.no\_CFRP} + E_{CFRP} \cdot I_{CFRP.el}}$$

$$n_2 := \frac{E_{CFRP} \cdot I_{CFRP.el}}{b_{CFRP} \cdot \left(E_s \cdot I_{el.no\_CFRP} + E_{CFRP} \cdot I_{CFRP.el}\right)}$$

$$n_3 := \frac{E_{adh} \cdot b_{CFRP}}{h_{adh}} \cdot \left(\frac{y_1}{E_s \cdot I_{el.no\_CFRP}} - \frac{y_2}{E_{CFRP} \cdot I_{CFRP.el}} \right)$$

$$\beta := \sqrt[4]{\frac{E_{adh} \cdot b_{CFRP}}{4 \cdot h_{adh}} \cdot \left(\frac{1}{E_s \cdot I_{el.no\_CFRP}} + \frac{1}{E_{CFRP} \cdot I_{CFRP.el}} \right)}$$

$$V(x_1) := \frac{P}{2}$$

$V(0 \cdot mm) = 4.25 \times 10^4 \text{ N}$

$$M(x_1) := P \cdot \frac{x_1 + a}{2}$$

$$D1(x_1) := \frac{d}{dx_1} \tau_1(x_1)$$

$$D3(x_1) := \frac{d^3}{dx_1^3} \tau_1(x_1)$$

$$D4(x_1) := \frac{d^4}{dx_1^4} \tau_1(x_1)$$

$$C_1(x_1) := \frac{E_{adh}}{2 \cdot \beta^3 \cdot h_{adh} \cdot E_s \cdot I_{el.no\_CFRP}} \cdot \left(V(0m) + \beta \cdot M(0m)\right) - \frac{n_3}{2 \cdot \beta^3} \cdot \tau_1(0m) + \frac{n_1}{2 \cdot \beta^3} \cdot \left(D4(x_1) + \beta \cdot D3(x_1)\right)$$

$$C_2(x_1) := \frac{-E_{adh}}{2 \cdot \beta^2 \cdot h_{adh} \cdot E_s \cdot I_{el.no\_CFRP}} \cdot M(0m) - \frac{n_1}{2 \cdot \beta^2} \cdot D3(x_1)$$

$$\sigma(x_1) := e^{-\beta \cdot x_1} \cdot \left(C_1(x_1) \cdot \cos\left(\beta \cdot x_1\right) + C_2(x_1) \cdot \sin\left(\beta \cdot x_1\right)\right) - n_1 \cdot D1(x_1)$$

$$\sigma_{max} := \sigma(0m)$$

$\sigma_{max} = 7.972 \times 10^3 \text{ MPa}$

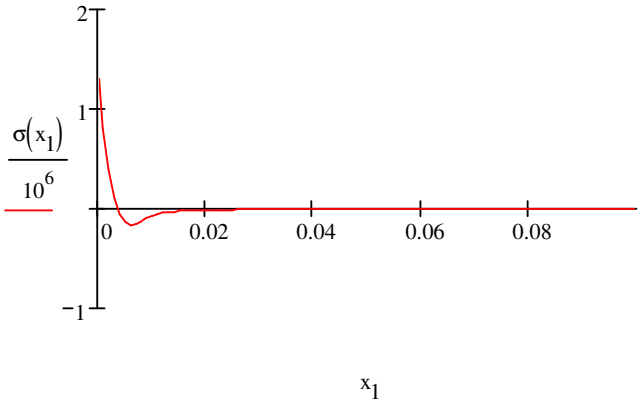
2
1
−1
σ(x1)
10^6
0
0.02
0.04
0.06
0.08
x1

Appendix B

Deflection in the Composite beam at 170kN

MathCAD file that calculates the deflection according to Smith and Teng[5]

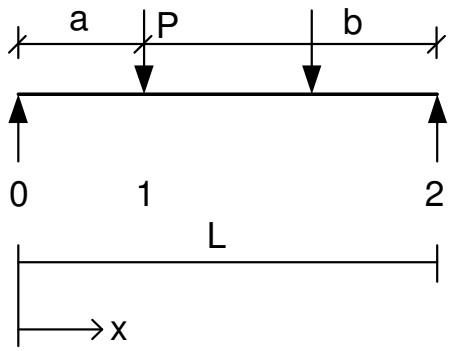

$P_{ref} := 148 \times 10^{3} N$

$L := 1.8 m$

$a_1 := 0.79 m$

$a_2 := L - a_1$

$a_2 = 1.01\ m$

$b_1 := L - a_1$

$b_2 := 0.79 m$

$EI := 5 \cdot 10^{6} \left(N \cdot m^2\right)$

Deflection at midpoint for two point loads

Expression 1:

$$y_{mitt\_Ref} := \frac{2P_{ref} \cdot a_1 \cdot \left(3 \cdot L^2 - 4 \cdot a_1^2\right)}{48 \cdot EI}$$

$y_{mitt\_Ref} = 7.038 \times 10^{-3}\ m$

$$y_{mitt} := \frac{2P \cdot a_1 \cdot \left(3 \cdot L^2 - 4 \cdot a_1^2\right)}{48 \cdot EI}$$

$y_{mitt} = 4.042 \times 10^{-3}\ m$

$$Ratio := \frac{y_{mitt}}{y_{mitt\_Ref}}$$

$Ratio = 0.574$

%%%%%%%%%%%%%%%%%%%%%%%%%%%%%%%%%%%%%%%

<u>Deflection at midpoint for one point load</u>

Expression 2:

$x_1 := 0, 0.01m .. a_1$

$x_2 := a_1 + 0.01m, (a_1 + 0.02m) .. L$

$$y_{0.1}(x_1) := \frac{P \cdot L \cdot b_1 \cdot x_1}{6 \cdot EI} \cdot \left(1 - \frac{b_1^2}{L^2} - \frac{x_1^2}{L^2}\right)$$

$$y_{1.2}(x_2) := \frac{P \cdot L \cdot a_1 \cdot (L - x_2)}{6 \cdot EI} \cdot \left(\frac{2 \cdot x_2}{L} - \frac{a_1^2}{L^2} - \frac{x_2^2}{L^2}\right)$$

$y_{0.1}(x_1) =$ (m)	$y_{1.2}(x_2) =$ (m)
0	$2.009 \cdot 10^{-3}$
$3.529 \cdot 10^{-5}$	$2.014 \cdot 10^{-3}$
$7.057 \cdot 10^{-5}$	$2.017 \cdot 10^{-3}$
$1.058 \cdot 10^{-4}$	$2.02 \cdot 10^{-3}$
$1.411 \cdot 10^{-4}$	$2.023 \cdot 10^{-3}$
$1.763 \cdot 10^{-4}$	$2.024 \cdot 10^{-3}$
$2.114 \cdot 10^{-4}$	$2.025 \cdot 10^{-3}$
$2.465 \cdot 10^{-4}$	$2.025 \cdot 10^{-3}$
$2.815 \cdot 10^{-4}$	$2.024 \cdot 10^{-3}$
$3.165 \cdot 10^{-4}$	$2.023 \cdot 10^{-3}$
$3.513 \cdot 10^{-4}$	$2.021 \cdot 10^{-3}$
$3.861 \cdot 10^{-4}$	$2.018 \cdot 10^{-3}$
$4.208 \cdot 10^{-4}$	$2.015 \cdot 10^{-3}$
$4.553 \cdot 10^{-4}$	$2.011 \cdot 10^{-3}$
$4.897 \cdot 10^{-4}$	$2.007 \cdot 10^{-3}$
$5.24 \cdot 10^{-4}$	$2.001 \cdot 10^{-3}$

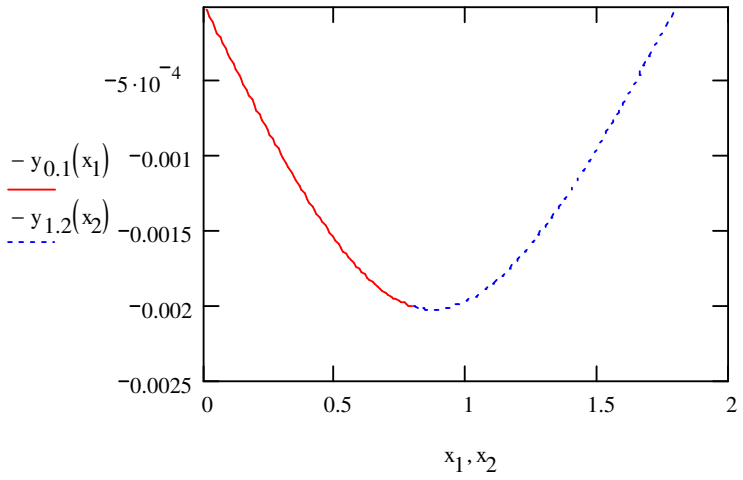

$x_3 := 0, 0.01m .. a_2$

$x_4 := a_2 + 0.01m, (a_2 + 0.02m) .. L$

$$y_{0.1}(x_3) := \frac{P \cdot L \cdot b_2 \cdot x_3}{6 \cdot EI} \cdot \left(1 - \frac{b_2^2}{L^2} - \frac{x_3^2}{L^2} \right)$$

$$y_{1.2}(x_4) := \frac{P \cdot L \cdot a_2 \cdot (L - x_4)}{6 \cdot EI} \cdot \left(\frac{2 \cdot x_4}{L} - \frac{a_2^2}{L^2} - \frac{x_4^2}{L^2} \right)$$

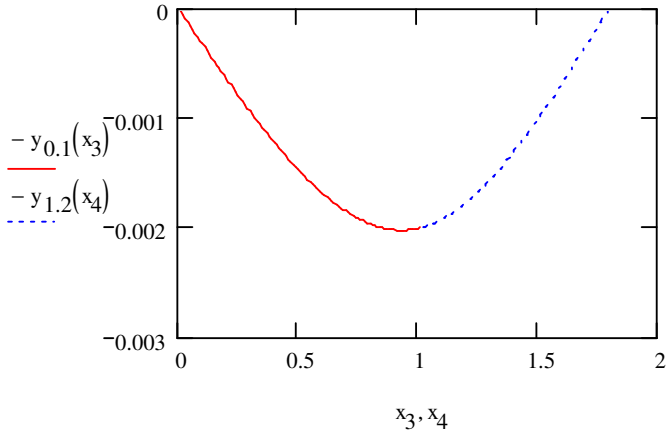

x_4 =		$y_{1.2}(x_4)$ =		x_3 =		$y_{0.1}(x_3)$ =	
1.02	m	$1.998 \cdot 10^{-3}$	m	0	m	0	m
1.03		$1.992 \cdot 10^{-3}$		0.01		$3.253 \cdot 10^{-5}$	
1.04		$1.984 \cdot 10^{-3}$		0.02		$6.505 \cdot 10^{-5}$	
1.05		$1.976 \cdot 10^{-3}$		0.03		$9.755 \cdot 10^{-5}$	
1.06		$1.967 \cdot 10^{-3}$		0.04		$1.3 \cdot 10^{-4}$	
1.07		$1.958 \cdot 10^{-3}$		0.05		$1.625 \cdot 10^{-4}$	
1.08		$1.948 \cdot 10^{-3}$		0.06		$1.949 \cdot 10^{-4}$	
1.09		$1.937 \cdot 10^{-3}$		0.07		$2.273 \cdot 10^{-4}$	
1.1		$1.925 \cdot 10^{-3}$		0.08		$2.596 \cdot 10^{-4}$	
1.11		$1.913 \cdot 10^{-3}$		0.09		$2.919 \cdot 10^{-4}$	
1.12		$1.9 \cdot 10^{-3}$		0.1		$3.24 \cdot 10^{-4}$	
1.13		$1.886 \cdot 10^{-3}$		0.11		$3.562 \cdot 10^{-4}$	
1.14		$1.872 \cdot 10^{-3}$		0.12		$3.882 \cdot 10^{-4}$	
1.15		$1.857 \cdot 10^{-3}$		0.13		$4.201 \cdot 10^{-4}$	
1.16		$1.842 \cdot 10^{-3}$		0.14		$4.52 \cdot 10^{-4}$	
1.17		$1.826 \cdot 10^{-3}$		0.15		$4.837 \cdot 10^{-4}$	

For two pointloads (superposition)

Appendix C

MATLAB® file for generation of the spring connectors between coincident meshes.

The file “aacradv.txt” is the file where the code that is to be pasted in the input file of the ABAQUS processor after the lines where the four initial corner connectors are described.

```
clear all

fid = fopen('aacradv.txt','a')

c=5;

% ----------------for the left 2mm grid---------------------------------

% half connectors left edge nodes

kc=[511:1:549];

kb=[592:-1:554];

   for i=1:39

fprintf(fid,'*Element, type=CONN3D2, elset=_Conn-%g_CnSet_\n%g, Part-1-1.%g, CFRP3-1.%g\n*Connector Section, elset=_Conn-%g_CnSet_, behavior=ConnProp-3\nCartesian,\n',c,c,kb(i),kc(i),c)

   c=c+1;

end

% half connectors top and bottom edge nodes

kc=[550:1:598   2

   510:-1:462  1];

kb=[553:-1:505  12

   39:1:87 3];

   for i=1:2

   for j=1:50

fprintf(fid,'*Element, type=CONN3D2, elset=_Conn-%g_CnSet_\n%g, Part-1-1.%g, CFRP3-1.%g\n*Connector Section, elset=_Conn-%g_CnSet_, behavior=ConnProp-4\nCartesian,\n',c,c,kb(i,j),kc(i,j),c)

   c=c+1;

end
```

```
end

% full connectors centre fill and right edge merged nodes

kc=[7151:1:9061 47:-1:9];

kb=[2878:1:4788 678:1:716];

   for i=1:1950

fprintf(fid,'*Element, type=CONN3D2, elset=_Conn-%g_CnSet_\n%g, Part-1-1.%g, CFRP3-
1.%g\n*Connector Section, elset=_Conn-%g_CnSet_, behavior=ConnProp-
5\nCartesian,\n',c,c,kb(i),kc(i),c)

   c=c+1;

end

% ----------------for the right 2mm grid---------------------------------

% half connectors right edge nodes

kc=[374:1:412];

kb=[639:1:677];

   for i=1:39

fprintf(fid,'*Element, type=CONN3D2, elset=_Conn-%g_CnSet_\n%g, Part-1-1.%g, CFRP3-
1.%g\n*Connector Section, elset=_Conn-%g_CnSet_, behavior=ConnProp-
3\nCartesian,\n',c,c,kb(i),kc(i),c)

   c=c+1;

end

% half connectors top and bottom edge nodes

kc=[373:-1:325   3

   413:1:461  4];

kb=[337:1:385  11

   255:-1:207 4];

   for i=1:2

   for j=1:50

fprintf(fid,'*Element, type=CONN3D2, elset=_Conn-%g_CnSet_\n%g, Part-1-1.%g, CFRP3-
1.%g\n*Connector Section, elset=_Conn-%g_CnSet_, behavior=ConnProp-
4\nCartesian,\n',c,c,kb(i,j),kc(i,j),c)
```

```
   c=c+1;

end

end

% full connectors centre fill

kc=[5240:1:7150 205:-1:167];

kb=[967:1:2877 600:1:638];

   for i=1:1950

fprintf(fid,'*Element, type=CONN3D2, elset=_Conn-%g_CnSet_\n%g, Part-1-1.%g, CFRP3-1.%g\n*Connector Section, elset=_Conn-%g_CnSet_, behavior=ConnProp-5\nCartesian,\n',c,c,kb(i),kc(i),c)

   c=c+1;

end

% ----------------for the centre 2mm x 5mm grid(advanced)---------------------------------

% half connectors right edge nodes(already considered)

% kc=[374:1:412];

% kb=[639:1:677];

%     for i=1:39

%         fprintf(fid,'*Element, type=CONN3D2, elset=_Conn-%g_CnSet_\n%g, Part-1-1.%g, CFRP3-1.%g\n*Connector Section, elset=_Conn-%g_CnSet_, behavior=ConnProp-3\nCartesian,\n',c,c,kb(i),kc(i),c)

%     c=c+1;

% end

% half connectors top and bottom edge nodes

kc=[48:1:166

   324:-1:206];

kb=[504:-1:386

   88:1:206];

   for i=1:2

   for j=1:119
```

```
fprintf(fid,'*Element, type=CONN3D2, elset=_Conn-%g_CnSet_\n%g, Part-1-1.%g, CFRP3-1.%g\n*Connector Section, elset=_Conn-%g_CnSet_, behavior=ConnProp-6\nCartesian,\n',c,c,kb(i,j),kc(i,j),c)

   c=c+1;

end

end

% full connectors centre fill

kc=[599:1:5239];

kb=[9429:-1:4789];

   for i=1:4641

fprintf(fid,'*Element, type=CONN3D2, elset=_Conn-%g_CnSet_\n%g, Part-1-1.%g, CFRP3-1.%g\n*Connector Section, elset=_Conn-%g_CnSet_, behavior=ConnProp-7\nCartesian,\n',c,c,kb(i),kc(i),c)

   c=c+1;

end

fclose(fid)
```

Appendix D

AutoCAD® file with the cross sectional details of the Composite beam.